Natural Resources Canada | Ressources naturelles Canada

DHP-TRACWin Manual

Canada

Sylvain G. Leblanc
Natural Resources Canada
Canada Centre for Remote Sensing

Centre Spatial John H. Chapman
6767, route de l'Aéroport
Saint-Hubert, Québec, Canada. J3Y 8Y9
Tel: 450-926-4646, Fax: 450-926-4449
Sylvain.Leblanc@CCRS.NRCan.gc.ca

Version 1.0.3 (10 October 2008)
DHP version 4.5.2
TRACWin version 4.1.1

Document made as part of the
ESS Reducing Canada's Vulnerability to Climate Change Program,
the ESS Health and Environment,
and the ESS Groundwater Program

This document replaces the
Digital Hemispherical Photography and the TRAC Manuals.

DHP-TRACWin Manual

Table of contents

1. Overview

The leaf area index (LAI) and its angular and spatial distributions are biophysical variables required in many ecological and climate models. In spite of their importance, the commercially available techniques for measuring these quantities are often less than adequate. Measurements have been made with commercial optical instruments such as the LAI-2000 Plant Canopy Analyzer (LI-COR), AccuPAR Ceptometer (Decagon), TRAC (3rd Wave Engineering) as well as hemispherical photography from films. However, these instruments are often combined to estimate correctly spatial and angular properties of leaf area index. This manual is intended for users of hemispherical photographs taken with a digital camera and the **DHP.exe/TRACWin.exe** programs. The manual contains the theory and field measurement protocol suggested to get the most out of using digital cameras for canopy structure extraction. Retrieval of LAI from this method has been compared with only a couple of site with allometric LAI based on destructive sampling, but it has been compared with TRAC measurements (Leblanc et al., 2005) and the TRAC technology has been validated in several studies (Chen and Cihlar, 1995a; Chen, 1996a, Chen et al., 1997; Kucharik *et al.*, 1997).

2. Field measurements protocol

Measurement of foliage density from any optical instruments is only a sampling of a greater foliage population and is generally done indirectly through the gaps in the canopy at a given point. Each plot and its rational to take the measurements are different, thus this is only a general guide to field measurements using digital cameras. **It must be strongly stated that using only one hemispherical photograph is not sufficient to accurately measure the LAI.**

2.1. The Plot

Plot size: Theoretically, the size of the plot should be at least 10 times the average distance between the major foliage structures such as crowns and crop rows. In forest stands, trees are usually found in clusters, so the plot needs to be substantially larger than a few tens of meters to consider the patchiness of the stands. Plots from 40x40 m^2 (e.g. Fig 2.1) to 100x100 m^2 are generally recommended.

For remote sensing validation purposes, plots are generally different than that of traditional forestry. If using a LANDSAT TM/ETM+ image with resolution of about 30m, plots should be at least 100 m from the edge of the forest stand to make sure that the opening is not included in the satellite pixel(s) corresponding to the plot, and it should be within a larger stand with similar attributes.

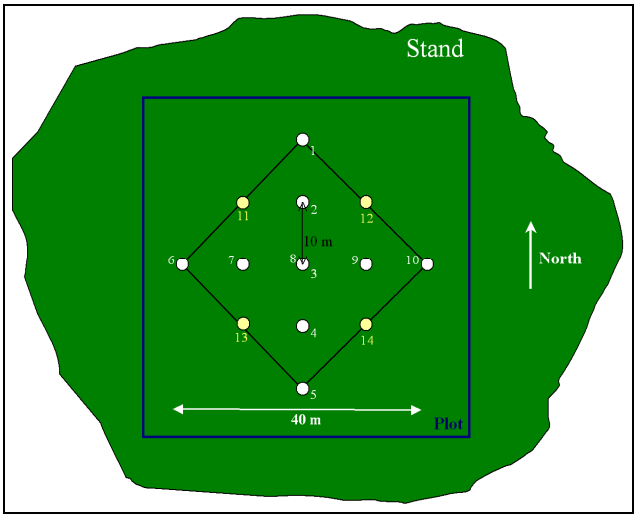

Figure 2.1 Minimum size suggested plot. White dots represent the main points to be taken while the yellow points are additional points that increase the sampling. Although the extend of the points is 40m, the actual plots is larger due to the footprint extend of the optical instruments (see Fig. 2.4). This scheme has a stronger weight at the centre of the plot.

2.2 Measurements on a slope:

Measurements on slopes require more care than flat surfaces. A plot should be chosen where the slope and aspect are near constant.

Two methods can be used for collecting hemispherical measurements on slopes:

1) Pointing the camera normal to the datum; or
2) Pointing the camera normal to the slope.

In case 1), the software used for the analysis will need to compensate for change of path length due to the slope and aspect of each pixel. In that case, the camera needs to be perfectly aligned to the slope and/or cardinal points Walter and Torquebiau (2000) have a correction for this purpose. The DHP software does not have the correction. It assumes that the photographs were taken normal to the slopes (Fig 2.2). In that case, for all pixels at a given radial distance from the centre, the view zenith angle is assumed the same.

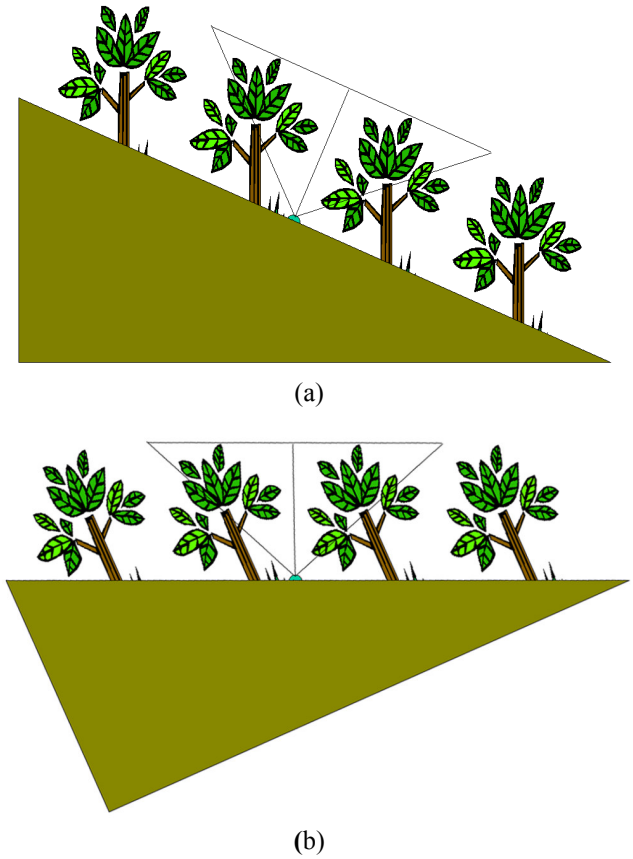

(a)

(b)

Figure 2.2: Measurements on a slope; a) the slope and the camera inclined, and b) the same image as in a), but tilted to show the measurements principle. By tilting the camera to the slope's normal, the measurements are then the same as on horizontal ground.

Figure 2.3: Stake used as a marker for camera placement

The absolute view zenith angle is different, but the effective view zenith angle, calculated from the slope's normal is the same. The view zenith angle is needed to calculate the path through the canopy ($Cos(\theta)$). When measurements are taken as in Fig. 2.2b, canopy closure estimates cannot be obtained from hemispherical photographs.

2.3 Camera orientation: for repeated measurements and a better assessment of light penetration through the canopy, the photographs should always be taken facing the same cardinal point, e.g, North up or down on the hemispherical photograph (Fig 2.1). When taking measurements without a compass, it is suggested to use the sun (if present) as a reference point.

2.4 Markers: For repeat measurements at a given plot, mark the measurements points every 10 m (or less for short vegetation plots) with an easily visible marker (flag or stake; see Figure 2.3). A cross pattern is usually good for sampling a plot (e.g. Fig. 2.1). Section 2.6 shows a more complex plot pattern.

2.5 Geometry of hemispherical photographs and footprint

Hemispherical photographs take a complete snapshot of the canopy, 360° in azimuth and 90° in zenith (Fig. 2.4). Each pixel of the photograph represents a different combination of view and zenith angle. Generally, the results are given only in term of zenith angle since an assumption of azimuthal symmetry is generally used. Because each pixel corresponds to a different path of the canopy, taking a single photograph is not statistically sound as conditions over the path length may be quite different, depending on the heterogeneity of the stand.

Figure 2.4: Geometry of a hemispherical photograph. The centre pixel is at the view zenith angle zero. A radial linear assumption is from the centre pixel to calculate the view zenith angle of each pixel. Relationships exist to correct lens imperfection that can change the linear assumption (Frazer et al., 2001).

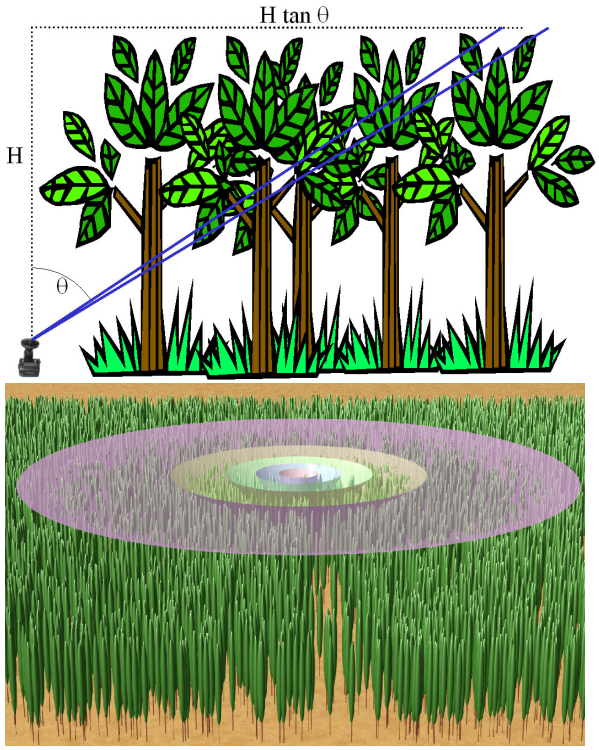

Figure 2.5: View zenith angle θ and footprint concept. The rings in (b) represents the five LAI-2000 concentric rings.

At a given view zenith angle θ, the top of canopy gaps are at tan(θ) times the canopy height from the camera (Fig. 2.5a). The canopy sampling is larger at larger zenith angle as a 360° annulus ring contains more pixels (Fig. 2.5b). To get a good sampling at the zenith, many photographs are needed. For view zenith angle larger than 30°, five photographs are usually sufficient (Leblanc et al., 2005).

2.6 Using DHP with other instruments

Although the footprint of the optical instruments is always important when taking optical measurements, it becomes critical when more than one instrument are used together.

To combine or compare instruments, care must be taken when a stand is not homogeneous. Figure 2.6 is a suggested plot that combined TRAC, LAI-2000 with a 90° or 180° view cap, hemispherical photographs (360° view) and typical forestry measurements. The size of 100x100m^2 was set for optimum comparison with LANDSAT TM 3x3 pixels (90x90m^2). This configuration allows a good coverage for each instrument with a minimum overlap and maximum LAI estimates from the trees inside the plot (for a stand with tree height around 10-20 m). On this configuration, the TRAC measurements need to be taken in the morning and LAI-2000 in the evening. The hemispherical photographs can be taken at any time that the sky condition is isotropic. Even this scheme allows trees outside the plot to be measured by some of the instruments, but the centre of the plot will have the maximum weight.

The suggested plot in Fig. 2.6 needs to be large enough for the sensors to see the same canopy. Comparison between TRAC and DHP clumping index from similar plot of only 25 by 25 metres squared compared poorly while large plots and long transects gave better results (Leblanc et al., 2005).

2.7 Taking the measurements:

Hemispherical Photographs should be taken under diffused sky, preferably near dawn or dusk. Uniform clouds can give a perfect diffuse sky, but the light intensity under uniform clouds is often very bright and can cause blooming on the photographs (Leblanc et al., 2005). Users with great experience in taking high contrast photographs should be able to take DHP under overcast sky. Sunlit conditions should be avoided at much as possible, especially for open canopies (see Fig. 2.7). The sub-pixel gap methodology used by DHP.exe does not work very well for digital photographs taken under sunlit conditions (Leblanc et al., 2005). A suggested method for exposure method based on Chen et al. (1991) and Zhang et al. (2005) is found in section 2.7.4.

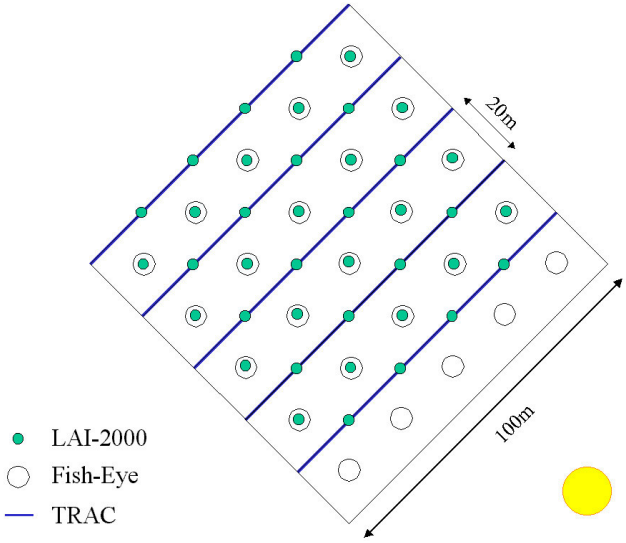

Figure 2.6 Suggested one ha plot (based on Bigfoot protocol and NASA SIBLAI project) where mid-day TRAC is combined with dusk LAI-2000 or hemispherical photographs.

Even photographs taken near dusk do not have perfect diffused conditions. When cloud and blue sky are present in an image, the blue and white sky being both saturated in the blue band, they often appear white in 8-bit blue channel (Fig. 2.8).

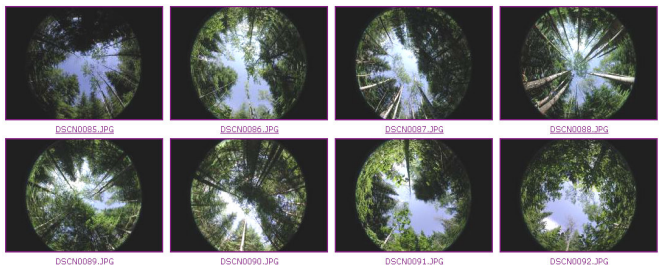

Fig. 2.7: Open canopies are very susceptible to sunlight conditions. Different parts of the canopy receive different level of solar radiation, making the thresholding difficult and unreliable.

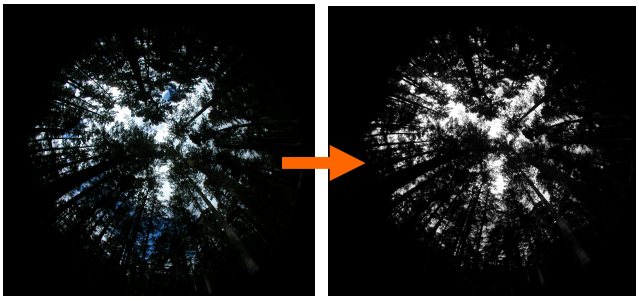

Fig 2.8: Colour photograph (left) taken under broken clouds condition near sunset. The blue channel (right) of the colour image does not show much variation in the sky pixel as both blue sky and clouds have high radiance in the blue band.

2.7.1 Deciduous

Deciduous species allows the measurements of plant area index and woody area index from optical sensors. The woody area index can be estimated from gap fraction before leaf-on or after leaf-off (Fig. 2.9).

2.7.2 Coniferous

For coniferous species, the woody material needs to be found from selective destructive sampling, or from tabled woody to total area ratio (Chen et al., 1997).

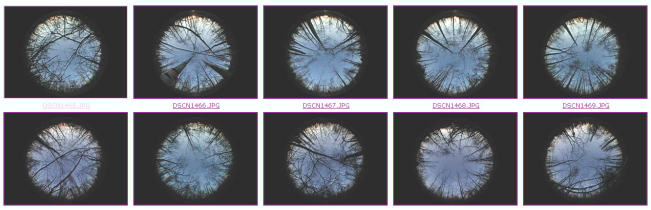

Fig 2.9 Digital hemispherical photographs taken before leaves emergence in a deciduous stand.

2.7.3 Agriculture, shrubland and grassland

Although theoretically feasible, it is not recommended to use large fish-eye devise for optical measurements of LAI in short canopies. The distance between the lens and the canopy may be too short; more care is needed to assure accuracy. Photographs may be taken looking down from above the short canopies. However, DHP was not designed to analyse hemispherical photographs taken looking downward. CAN-EYE (http://www.INRA.fr/eyecan/) is suggested for this type of analysis.

2.7.4 Measurements Step-by-Step (based on Fluxnet Canada protocol for CoolPix 4500, Leblanc and Chen, 2004)

a) The camera needs to be set to "manual" mode.

- Make sure the camera is in **fine mode (Jpeg),** with the highest resolution **(e.g., 2272x1704 for CoolPix 4500).**

b) Install the camera on the tripod.

c) Before entering the forest, the following procedure is recommended to determine the **Exposure:** Choose a large open area that is close to the photo site but large enough for sky exposure up to 75 degree zenith angle in all directions, and use the camera to measure the exposure

with the fisheye lens. The camera should be pointed to the zenith of the sky (levelled). To find the exposure, press the shutter button halfway, and then hold on. The exposure indicator will appear on screen, turn the command dial left or right to make the middle small square appear solid and others on both sides empty. The exposure (in terms of the shutter speed as the aperture is already fixed when the camera is set in the Fisheye1 mode) is the exposure that shows the sky as a grey body (17% of the brightness) on the photograph.

d) Go to Point #1 on the plot, level the camera if not on a slope. On a slope, incline the camera so that the measurements are taken normal to the slope.

e) The height of the camera is dependent on the canopy condition. For mature stands without important understory, the camera can be at breast height (1.3 m). When an important understory is present, the camera should be above the understory if only overstory LAI is needed. A series of photographs under the understory should also be taken when possible to assess the understory LAI. However, other instruments, such as the LAI-2000 or the Ceptometer, may be better suited to assess understory LAI.

f) To take fisheye photographs in forests, the exposure must be adjusted. The correct exposure is to make the sky appear white, so you need to allow 2.5 stops more exposure (rounded to 2 stops) than the speed-reading taken outside the forest. For example, if the sky exposure time is 1/500", the exposure in forests should be 1/125". A simple way in practice is to increase the exposure by 2 stops by turning the command dial left twice after getting the sky exposure outside forest and make it fixed.

g) Take the photograph

- After taking a photograph, go to "play" mode by pressing the "play button" (for CoolPix 4500, it looks the same as on a VCR) twice. Turn the command dial until you reach the histogram mode. The upper left of the viewer should reveal the photographs you took. If you have saturation, the portion of the image saturated will flash. The goal is to allow some saturation near in the largest opening (often near zenith), far from canopy elements.

- If case of doubt, take one photo at the setting that you feel is right, then take two others with more and less light by adjusting either the speed, or aperture to obtain different light readings.

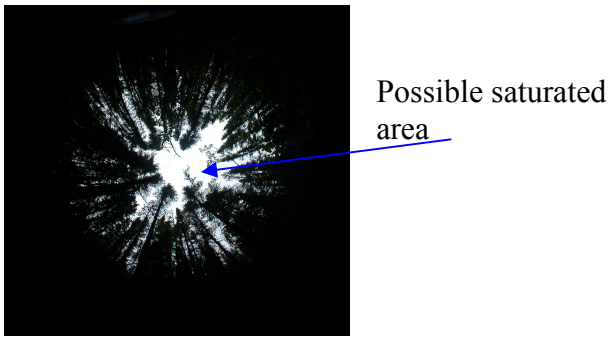

Figure 2.10, example of a digital hemispherical photograph. Saturation should only be found near the zenith, far from the foliage.

h) Go to next point and repeat from **f.** To simplify future re-analysis that may come from new theory, always take the photographs in the same order: Northern point, going south, and then from western point, going east. Very often, the settings found at one points can be used for all photographs in a plot.

To simplify the analysis, a datasheet should be filled for each photograph, for example:

- **Site**: the name or code of the site or tower.
- **Plot**: A plot name or number to identify the specific plot
- **Point**: the point number based on Fig 1.
- **Date**: the date the photograph was acquire
- **Time**: exact time of a given point photographs
- **Flash Card**: The name/number of the Flash card (e.g. 3.4)
- The **filename** of the photographs (e.g. DSCN0201)
- **Notes**: any comments of notes about a particular photographs (e.g. some clouds, low batteries, high saturation, less light, more light, meter at zero, etc)

Since each photograph keeps the camera setting used (for example, often embedded in the jpeg file), there is no need to write them down.

3. Data analysis

Only a few steps are needed to do the analysis. The operator has decisions to make only in the thresholding part. Although some automated thresholding methods exist (Jonckheere et al., 2005) none had enough success so far to be considered as an option in DHP.exe that requires multiple thresholds for which no automated methods have been developed. The remaining analysis has been automated when possible**.** The software always indicates the version in the files created to facilitate future updates.

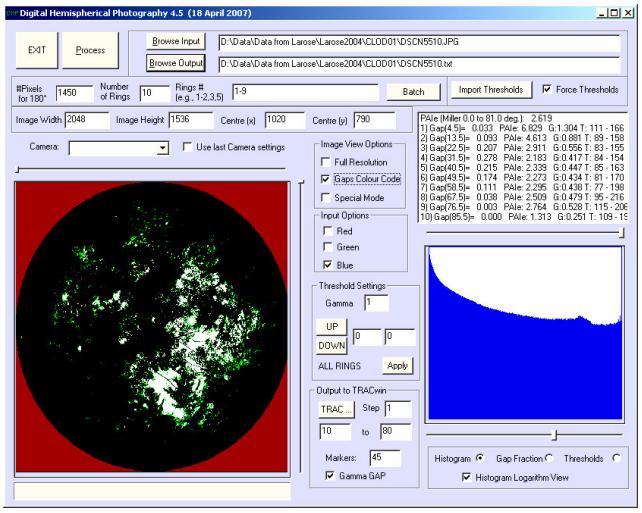

Figure 3.1: Screen shot of DHP software 4.5 developed at Canada Centre for Remote Sensing.

Steps (more details to follow in next sections):

1. Put all DHP's from a given plot into a new directory. For proper statistics, **you should have at least 5 images per plot.**

2. DHP can open the following image formats: RAW single 8-bit image without headers, jpeg, png, pcx, bmp, tga, and gif (using the corona library http://corona.sourceforge.net/) . You need to specify the channel (s) you want to use (red, green, blue) before opening the images (except when opening a raw image) and the gamma correction factor that was applied to the image (see section 6 for a discussion on gamma correction). Use gamma of 2.2 when gamma is not known. It is the sRGB default gamma value. The "thresholds interpolated" option has been removed since version 4.0.

   a) If **Force Thresholds** is disabled, the software will find thresholds based on some criteria described in Leblanc et al., 2005. These thresholds are not usually the ones needed. Inspect the image (shades of green) to assess the thresholds automatically found. Change the thresholds as necessary and repress "**Process**".

   b) Extract TRAC-like profile by pressing "**TRAC…**" button (We suggest Step 1, 10 to 80, NORMALIZED).

3. Redo step 2 with all other images from the plot to be analysed.

4. In TRACWin (version 4 and up), used the DHP mode and press "setup" to choose the directory containing the original images and the folders TXX created by DHP. Chose also the VZA with either one or all photographs to be processed.

If you camera is not on the list, or if you have different values for the image geometry, you can use the "Use last settings" to keep the same image settings when opening a new file. You can also send the camera specification to sylvain.leblanc@ccrs.nrcan.gc.ca and a special version of DHP.exe can be made for you.

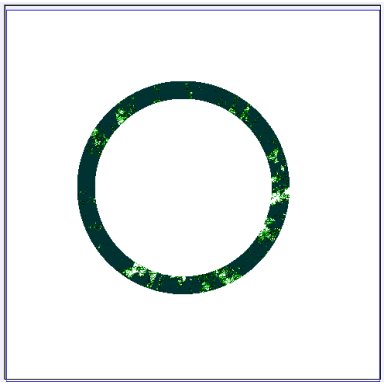

Figure 3.2: Annulus ring #6 (46-54°). Pure canopy pixels are in black; pure gap pixels in white; and mixed canopy-gap pixels are colour coded in shades of green.

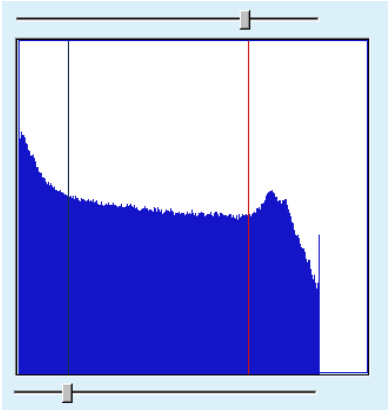

Figure 3.3: Histogram of annulus ring # 6 from Figure 3.2. The red line represents the high threshold (DN_{Max}) and the

dark green line the low threshold (DN_{Min}) is used to separate pure and mixed pixels.

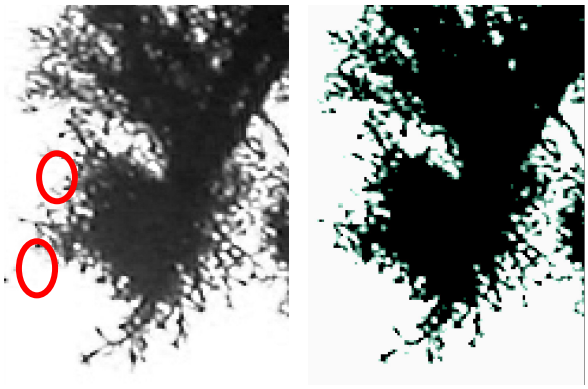

Fig. 3.4: Thresholding effect on a DHP. Only edges or the original (leaf-hand side) raw image are colour coded in green (right-hand side) in the view are of DHP.exe. Even with the best thresholds, it is possible that some foliage element will disappear (see circles).

The following is an example of the final output of the DHP analysis.

```
gap( 4) = 1.000000  (    14002    14002) PAIe:    0.0000
gap(13) = 1.000000  (    43057    43057) PAIe:    0.0000
gap(22) = 1.000000  (    70866    70866) PAIe:    0.0000
gap(31) = 1.000000  (   100745   100745) PAIe:    0.0000
gap(40) = 1.000000  (   127670   127670) PAIe:    0.0000
gap(49) = 0.999935  (   158431   158441) PAIe:    0.0001
gap(58) = 0.918539  (   169513   184546) PAIe:    0.0901
gap(67) = 0.763795  (   165042   216081) PAIe:    0.2106
gap(76) = 0.457511  (   110442   241398) PAIe:    0.3783
gap(85) = 0.155456  (    42556   273753) PAIe:    0.3245

G( 4) =   0.000 (  0.000)
G(13) =   0.000 (  0.000)
G(22) =   0.000 (  0.000)
G(31) =   0.000 (  0.000)
G(40) =   0.000 (  0.000)
G(49) =   0.000 (  0.000)
G(58) =   0.296 (  0.371)
G(67) =   0.692 (  0.867)
G(76) =   1.244 (  1.558)
G(85) =   1.067
PAIe  :  0.121
```

Thresholds:	133	163	133	163	130	160	126	156	112	145	110	131	89	117	77	101	66	86	52	74
DN:0	0	0	0	0	0	0	0	0	0	0	0	0	0	19	0	0				
DN:1	0	0	0	0	0	0	0	0	0	0	0	1	5	2	5					
DN:2	0	0	0	0	0	0	0	0	0	0	1	6	8	27						
DN:3	0	0	0	0	0	0	0	0	0	0	0	8	18	327						
DN:4	0	0	0	0	0	0	0	0	0	0	0	10	95	1726						
DN:5	0	0	0	0	0	0	0	0	0	0	4	19	564	5683						
DN:6	0	0	0	0	0	0	0	0	0	0	0	67	1592	11975						
...																				
DN:123	0	0	0	0	0	0	0	0	0	0	130	3412	1278	1105						
DN:124	0	0	0	0	0	0	0	0	0	0	158	3505	1244	1101						
DN:125	0	0	0	0	0	0	0	0	0	0	191	3439	1191	972						
DN:126	0	0	0	0	0	0	0	0	0	1	239	3665	1253	942						
DN:127	0	0	0	0	0	0	0	0	0	0	325	3489	1431	1026						
DN:128	0	0	0	0	0	0	0	0	0	0	468	3430	1340	995						
...																				
DN:199	752	1148	1019	1007	564	1029	180	0	0	0										
DN:200	758	1151	858	897	623	1023	108	0	0	0										
DN:201	716	1091	864	874	603	883	73	0	0	0										
DN:202	702	1110	891	862	614	821	47	0	0	0										
DN:203	761	980	963	989	628	698	34	0	0	0										
DN:204	985	999	1048	1010	580	645	25	1	0	0										
DN:205	1055	933	1116	1094	673	566	14	0	0	0										
DN:206	960	943	1178	1099	611	574	7	0	0	0										
....																				
DN:242	0	0	0	0	0	0	0	0	0	0										
DN:243	0	0	0	0	0	0	0	0	0	0										
DN:244	0	0	0	0	0	0	0	0	0	0										
DN:245	0	0	0	0	0	0	0	0	0	0										
DN:246	0	0	0	0	0	0	0	0	0	0										
DN:247	0	0	0	0	0	0	0	0	0	0										
DN:248	0	0	0	0	0	0	0	0	0	0										
DN:249	0	0	0	0	0	0	0	0	0	0										
DN:250	0	0	0	0	0	0	0	0	0	0										
DN:251	0	0	0	0	0	0	0	0	0	0										
DN:252	0	0	0	0	0	0	0	0	0	0										
DN:253	0	0	0	0	0	0	0	0	0	0										
DN:254	0	0	0	0	0	0	0	0	0	0										

The first part:

```
gap(58) = 0.918539  (   169513    184546) Le:    0.0901
```

has the mean gap fraction, with number of pixels used for the analysis (e.g. 169513/ 184546 = 0.918539), and effective PAI (PAIe) assuming random (spherical) leaf angular distribution. The second part has an estimate of G(θ) (eq. 5.1) based on the effective PAI. The PAIe given: PAIe: 0.121 is based on Miller (1967). The thresholds used follow with the DN histogram for each annulus ring.

3.1 How to set up the thresholds manually?

To change the thresholds found by DHP, you can either move the slider (Fig. 3.3) or enter manually the values and press R:

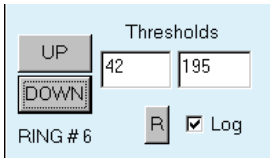

The "UP" and "DOWN" buttons are used to view different annulus rings. The thresholds for each ring can be set by entering the numerical values here and pressing "R". The log option is useful to view histogram in logarithm scale.

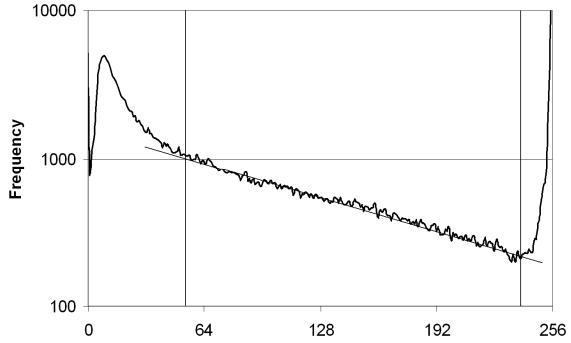

Fig. 3.5 Example of a histogram (θ = 58°) and the thresholds.

The thresholds are chosen from the histogram (e.g Fig 3.4). The lower thresholds is found were the histogram start its linear behaviour in logarithmic scale while the higher threshold is found where the linear behaviour ends The green coded image (e.g. Fig. 3.2.) can then be used to verify that all canopy elements are either black, or in shades or green for mixed canopy-sky pixels. Results for each image can be seen in the results window:

```
PAIe (Miller 0.0 to 81.0 deg.):  2.168
1) Gap(4.5)=  0.415  PAIe: 1.753  G:0.404 T: 138 - 158
2) Gap(13.5)=  0.173  PAIe: 3.409  G:0.786 T: 138 - 155
3) Gap(22.5)=  0.146  PAIe: 3.560  G:0.821 T: 136 - 157
4) Gap(31.5)=  0.131  PAIe: 3.470  G:0.800 T: 136 - 159
5) Gap(40.5)=  0.170  PAIe: 2.694  G:0.621 T: 139 - 157
6) Gap(49.5)=  0.181  PAIe: 2.222  G:0.513 T: 134 - 156
7) Gap(58.5)=  0.195  PAIe: 1.708  G:0.394 T: 131 - 153
8) Gap(67.5)=  0.114  PAIe: 1.662  G:0.383 T: 137 - 157
9) Gap(76.5)=  0.086  PAIe: 1.144  G:0.264 T: 121 - 168
10) Gap(85.5)=  0.013  PAIe: 0.680  G:0.157 T: 152 - 174
```

The PAIe displayed at the top is based on Miller's integration over the angles range (e.g. 1-9, 0-81° by default). For each annulus ring, the gap fraction, the effective PAI, the projection coefficient *G* and the thresholds are displayed. All these values can be found in the file output along with the histograms.

Instead of the histogram, the mean gap fraction can be plotted by selecting Gap fraction in:

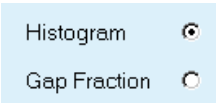

Choice of histogram or gap fraction viewing. The gap fraction view is from each annulus ring average.

Automated thresholding

Find more occurring DN below 75 and above 90 for $DN_{MIN}(\theta)$ and $DN_{MAX}(\theta)$, respectively. Then verify the values with:

If $DN_{MIN}(\theta)$ is not within 2.5 standard deviations of the mean for all angles, then
$DN_{MIN}(\theta) = DN_{MINMean} \pm 2.5 * \sigma_{MIN}$;

If $DN_{MAX}(\theta)$ is not within 2.5 standard deviations of the mean for all angles, then
$DN_{MAX}(\theta) = DN_{MAXMean} \pm 2.5 * \sigma_{MIN}$;

Where σ is the standard deviation of the DN's. The peak is not the value needed, so the following transformation is done:

$DN_{MIN}(\theta) = DN_{MIN}(\theta) + 40$,
$DN_{MAX}(\theta) = DN_{MAX}(\theta) - 20$.

If $DN_{MIN}(\theta)$ is greater than $DN_{MAX}(\theta)$, then
$DN_{MIN}(\theta) = DN_{MAX}(\theta) - 30$.
Finally, the software makes sure that the max and min DN are with 0 and 255.

3.2 Full Resolution mode

Versions 1.5 and up have a full resolution mode that allows the display of all pixels. It can be done full display or per ring (see Fig. 3.6)

The special mode allows you to display annulus rings coded in shades of green while displaying the rest of the image in shades of grey.

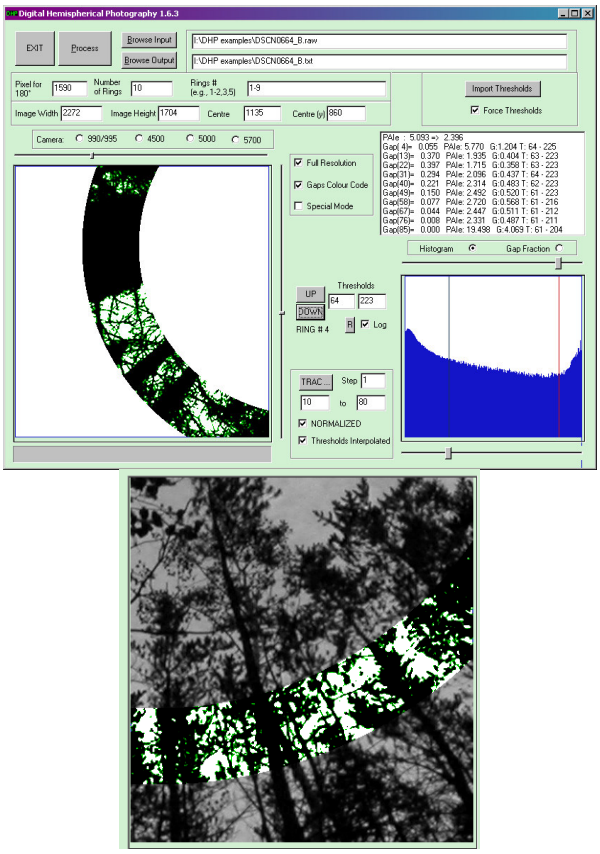

Figure 3.6: Examples of full resolution mode (up) and full resolution with special mode (down). In the special mode, the other rings than the one the user wants to work on, are displayed in the original 256 shades of grey.

3.3 Extracting the TRAC-Like profile

The "**TRAC…**" button is used to extract TRAC-like series to be analysed in TRACWin (Leblanc et al., 2002). The normalized option should be used all the time unless required by specific study. The range of view zenith angle extracted is set in this part and the step is the zenith angular steps between two extracted TRAC-like profiles. The defaults are from 10 to 80° with step of 1° and markers every 45°. This extracts profile of one pixel in the zenith range, corresponding often to less than 0.1 degrees. If **Gamma Gap** is off, Gamma is automatically set to 1.0. See section 6 for more details on gamma.

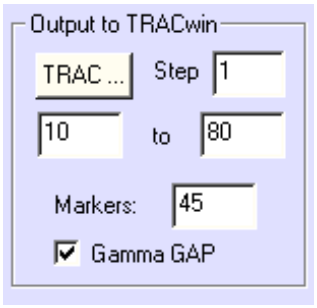

The TRAC. button creates a file named "TRACWin.dhp" that is used by TRACWin in the DHP mode. Fig. 3.5 shows a small annulus centred at 55° with its extracted (not normalized) first 45° TRAC-like profile. Fig. 3.6 shows two profiles One complete photograph), one at 10 degrees and one at 57° from a boreal black spruce stand.

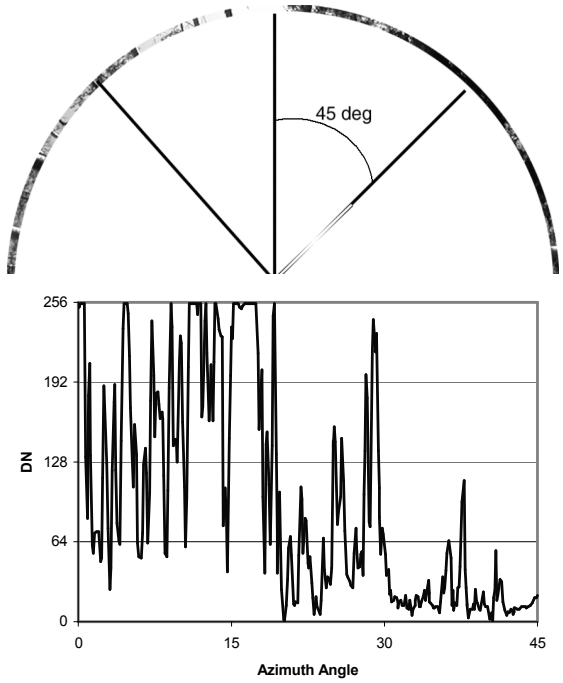

Figure 3.7: a) Hemispherical photograph arc near view zenith angle of 55°. An example of TRAC-like measurements in a mixed spruce aspen stand near Smooth Rock Fall, Ontario. The profile is extracted from the 45° arc.

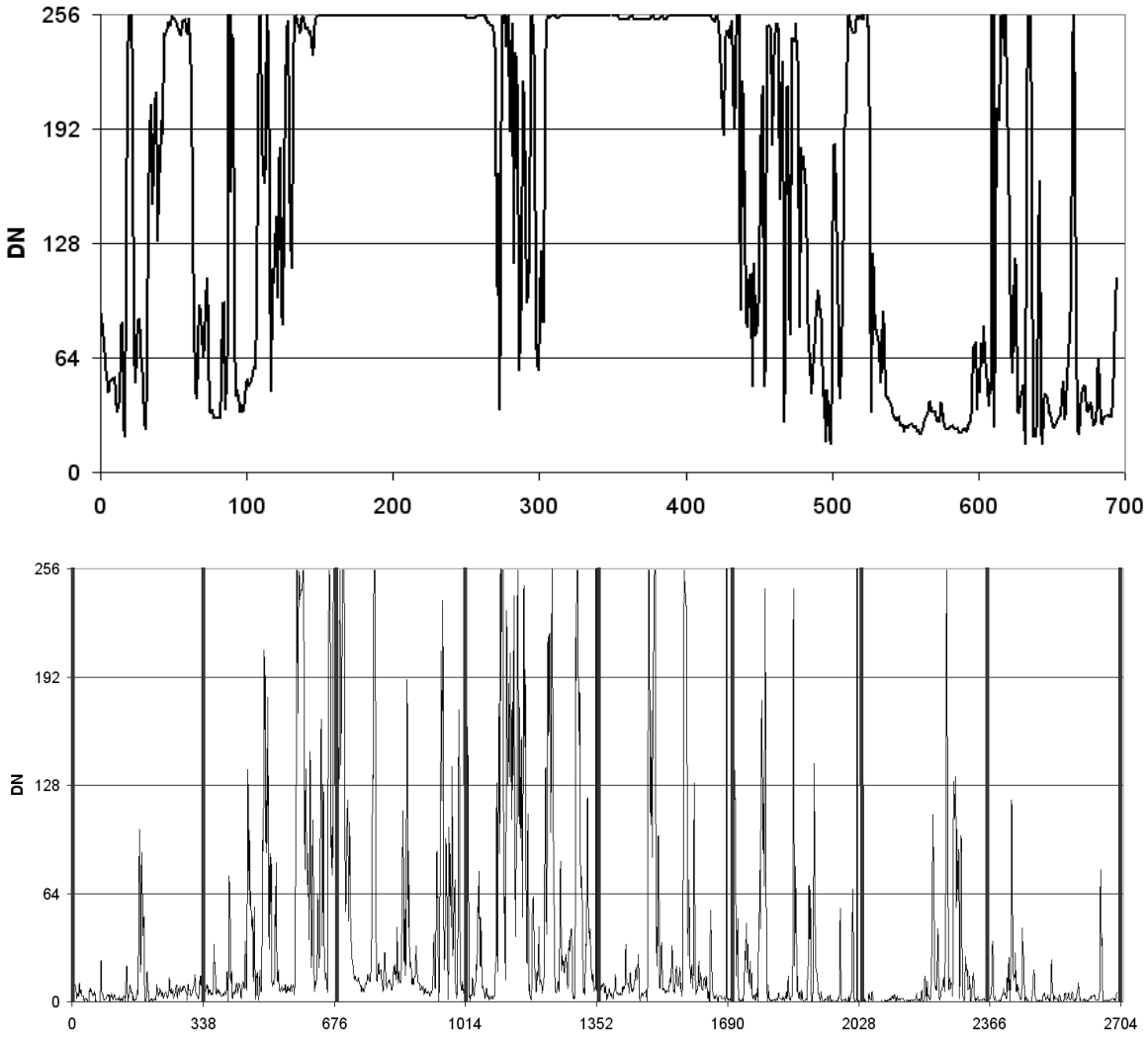

Figure 3.8: TRAC-like DN profiles from one digital hemispherical photograph for a) view zenith angle 10° and b) view zenith angle 57°. The profiles are in one-pixel intervals in the zenith angle resolution.

4.0 TRACWin

TRACWin can be used for TRAC data or outputs from DHP.exe. TRACWin is very easy to use with few instructions in TRAC mode and is completely automated in DHP mode if the output from DHP.exe is used. DHP output can be open in TRAC mode for some special analysis.

What is needed before processing?

- You need to have a TRAC-like file made with DHP.exe.
- You need the needle-to-shoot ratio. For flat leaves, the needle-to-shoot ratio is one. For coniferous forests, you need a needle-to-shoot ratio greater than unity in order to consider clumping at scale less than the shoot in coniferous trees. Some typical values (Gower *et al*., 1999):
  - Black spruce (*Picea mariana*): 1.30-1.40;
  - Jack pine (*Pinus Banksiana*): 1.20-1.40;
  - Red pine (*Pinus resinosa)*: 2.08,
  - Scots pine (*Pinus sylvestris*): 1.75;
  - Douglas Fir (*Pseudotsuga menziesii*): 1.77

- You need to know the woody to total area ratio. A value of zero means that no woody material was "seen" by TRAC. Typical values (Gower *et al*., 1999):
  - Black spruce (*Picea mariana*): 0.12-0.17;
  - Jack pine (young) (*Pinus Banksiana*): 0.03-0.05;
  - Jack pine (old) (*Pinus Banksiana*): 0.11-0.34;
  - Red pine (*Pinus resinosa)*: 0.07,
  - Douglas Fir (*Pseudotsuga menziesii*): 0.08
  - Aspen (*Populous tremuloides*): 0.21-0.22
  - Oak-hickory: 0.11
  - Sitka spruce: 0.23

To use the automated mode, check the DHP option (Figure 4.1). Then click on **Setup** (Figure 4.1). This will open a new Window (Figure 4.2). To setup the DHP analysis, enter the directory name where the TXX (e.g. T10, T11) directories of your plots are located.

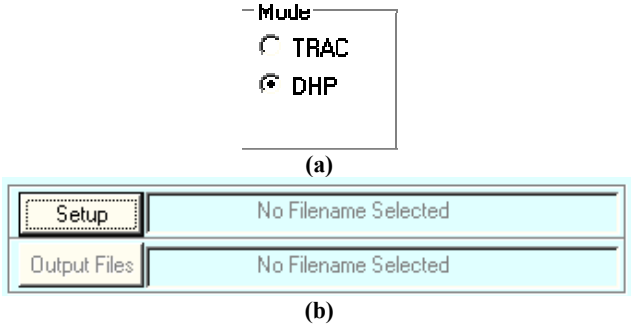

Figure 4.1: Mode selection for TRACWin (version 4.5 and up) and setup button.

This will automatically show you the available range of VZA and the images used for that plot. In version 4.5, you can choose either: all images or a single image, and all VZA, a single VZA, or a preset range from 55 to 60°. More choices will be available in future versions. Press **Process** and the program will start the analysis.

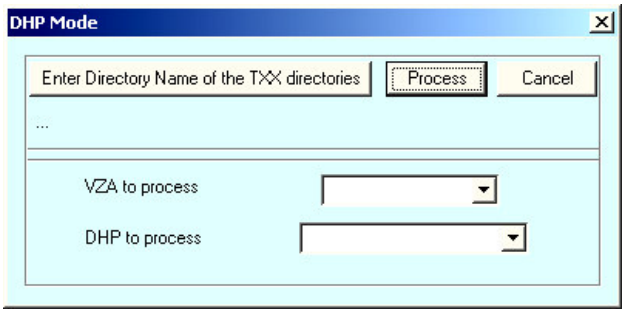

Figure 4.2: DHP mode setup dialog

The program also creates many files *.lai, *.fmr and *.pfl in every subdirectory. The right hand side of TRACWin (Figure 4.3) will reveal the segments (or blocks) with the number of measurements in each of those segments. A segment represents an arc as defined in DHP.exe.

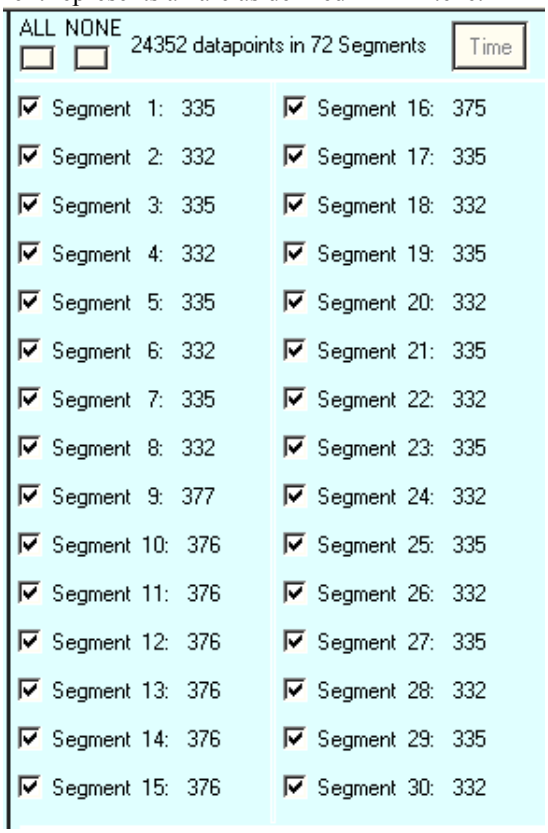

Figure 4.3: Right-hand-side of TRACWin where the segments number and number of data points appear. In DHP mode, the Time option is invalid. In this mode, each segment represents 45 degrees in azimuth.

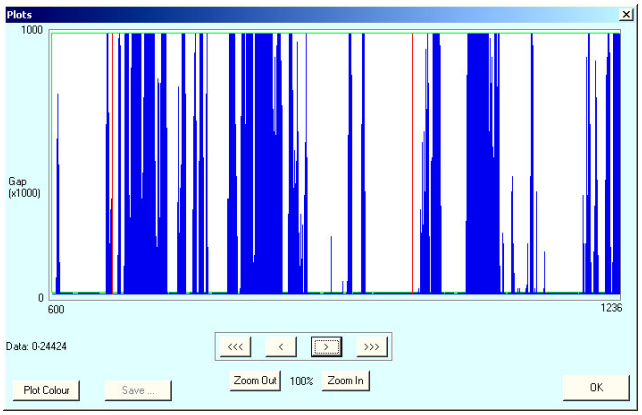

Figure 4.4: TRAC-like gap fraction profile (zenith 57°) normalized between 0 and 1000.

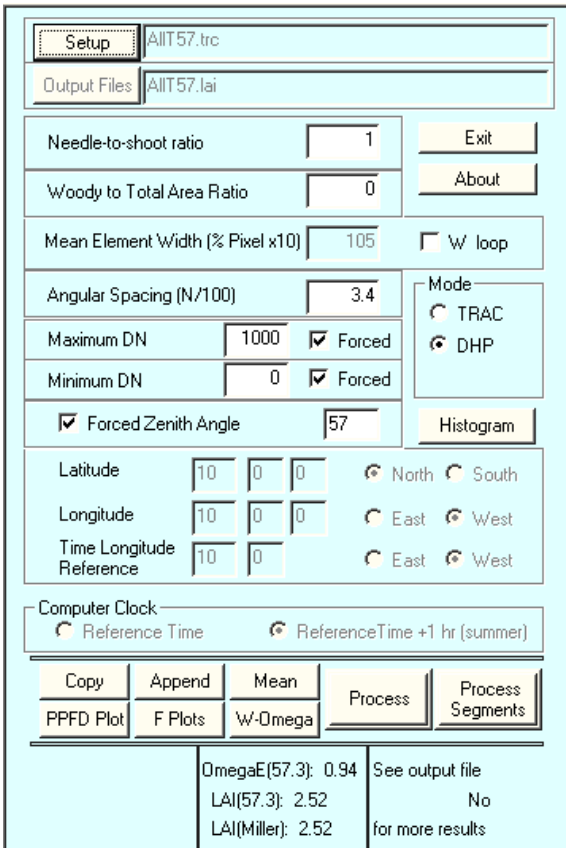

Figure 4.5: Left hand side of TRACWin where the input parameters are entered. When DHP mode is used, the spacing between markers is set automatically to the average number of data points (pixels) in a segment divided by 100 (e.g. 294/100 = 2.94), The zenith angle is set based on the directory name (e.g. T55 gives 55 degrees) and the below and above thresholds are set to 0 and 1000, respectively. The W loop is automatically selected in DHP mode. Button used to access the different options/capabilities of TRACWin.

TRACWin options:

Process and Process Segments:

Figure 4.7 shows what results appear when you press **Process**. The date, the time of acquisition, an estimate of W_p (mean element width based on the data using the P approach, the mean contact number **Kmean**, the **gap fraction**, the clumping index (**OmegaE**) at scale larger than the element casting the shadows, the solar zenith angle (**SZA**), the effective PAI and the LAI.

Copy Segment(s):

Useful if you want to break a large data file into smaller files. Just choose the segments you want to copy and press the Copy Button. It will ask you for a file name.

Append Segment(s):

Useful to append two transects of the same plot to be analysed together. It allows TRACWin to be a TRAC file manager with the combined Copy and Append segments options.

Compute **Mean** of Segment (s):

Useful for computing the mean PPFD of a segment. If you have a reference segment, you can then use that value as the maximum PPFD.

F Plots:
Plots F_m, F_{mr} *and* F_r. It does not display the number on the axis yet.

Figure 4.7: F_m, F_{mr} *and* F_r curves based on data and typical element size.

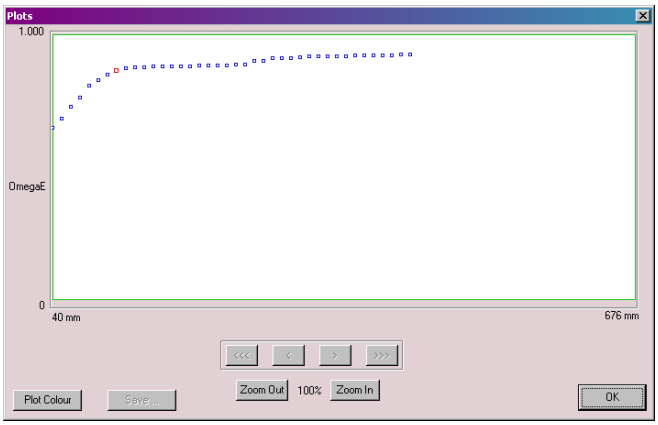

Figure 4.8: W-OmegaE: Plots the variations of the clumping index (OmegaE) versus the input foliage width. The red square represent the clumping index based on the foliage width on the main dialog box.

4.1. TRACWin Results

In DHP mode, complete results are found in the*.tab file. The output filename is based on the folder, zenith angles, and photographs used.

```
File C:\Documents and Settings\sleblanc\Desktop\Sims\T001-251\Case 010\CLX-15_All_10-70.tab created on January 23, 2008
TRACWin Windows Version 4.1.1
Alpha: 0.000 Gamma: 1.000
Angle GFCI(CC) CI(LX) CI(CLX) CI(CCW) PAIe LAI(CC) LAI(LX) LAI(CLX) LAI(CCW) G(CLX) W
10 0.676 0.786 0.393 0.376 0.997 0.771 0.98 1.96 2.05 0.77 0.26 290.9
11 0.665 0.659 0.342 0.321 1.000 0.801 1.22 2.34 2.50 0.80 0.31 429
12 0.638 0.711 0.363 0.336 0.932 0.880 1.24 2.42 2.62 0.94 0.33 307
13 0.603 0.67 0.396 0.351 0.996 0.985 1.47 2.49 2.80 0.99 0.35 453

.....

55 0.129 0.862 0.686 0.556 0.816 2.347 2.72 3.42 4.22 2.88 0.53 153.2
56 0.121 0.887 0.696 0.568 0.978 2.360 2.66 3.39 4.15 2.41 0.52 161.3
57 0.112 0.883 0.696 0.596 0.883 2.382 2.70 3.42 4.00 2.70 0.50 157.9
58 0.101 0.892 0.723 0.598 0.844 2.431 2.73 3.36 4.07 2.88 0.51 154.2
59 0.091 0.868 0.706 0.598 0.941 2.471 2.85 3.50 4.13 2.63 0.52 132.8
60 0.086 0.871 0.697 0.697 0.926 2.455 2.82 3.52 3.52 2.65 0.44 125.4
61 0.08 0.899 0.726 0.612 0.773 2.450 2.72 3.38 4.00 3.17 0.50 141.1
62 0.072 0.893 0.732 0.617 0.937 2.472 2.77 3.38 4.01 2.64 0.50 132.9
63 0.064 0.916 0.713 0.618 0.931 2.50 2.73 3.50 4.04 2.69 0.51 149.1
64 0.055 0.904 0.744 0.64 0.983 2.546 2.82 3.42 3.97 2.59 0.50 142.4
65 0.047 0.91 0.738 0.648 0.952 2.589 2.84 3.51 3.99 2.72 0.50 140.1
66 0.04 0.934 0.758 0.671 0.854 2.616 2.80 3.45 3.90 3.06 0.49 169.1
67 0.033 0.956 0.774 0.774 0.99 2.66 2.78 3.44 3.44 2.69 0.43 174.9
68 0.024 0.955 0.777 0.688 0.966 2.798 2.93 3.60 4.06 2.90 0.51 166.9
69 0.017 0.964 0.797 0.729 0.991 2.919 3.03 3.66 4.00 2.95 0.50 176.1
70 0.012 0.969 0.821 0.763 0.936 3.001 3.10 3.66 3.94 3.21 0.49 179.5
================================================================================

================Results==================

   55-60(57.3) Miller (10-70)

PAIe: 2.41 2.16
LAI(CC): 2.74 2.55
LAI(LX): 3.44 3.35
LAI(CLX): 4 3.98

CI(CC) 0.877 0.845
CI(LX) 0.701 0.643
CICLX) 0.602 0.542
==========================================
OPENNESS(10-70): 0.214
Crown Closure = 0.446
```

Alpha: (α) woody to total area ration used.
Gamma: (γ) needle-to-shoot area ratio used.

Column:

Angle: view zenith angle.
GF: gap fraction
CI(CC): Clumping index method CC (Chen and Cihlar)
CI(LX): Clumping index method LX (Lang and Xiang)
CI(CLX): Clumping index method CLX (Leblanc et al, 2005)
CI(CCW): Clumping index from Walter et al. (2003)'s method similar to CC.
PAIe: Effective Plant Area Index (also referred to as Effective LAI)
LAI(CC): LAI with clumping index CC and $G(\theta)$ =0.5.
W: Projected element used in CC method.
LAI(LX): LAI with clumping index LX and $G(\theta)$ =0.5.
LAI(CLX): LAI with clumping index CLX and $G(\theta)$ =0.5.
LAI(CCW): LAI with clumping index CCW and $G(\theta)$ =0.5.
G(CLX): Projection coefficient found with LAI(CLX)

Results at bottom of the file are given with average between 55-60° and on view zenith angle used using Miller's theorem:

PAIe: this is the effective plant area index that includes wood and foliage element (leaves for deciduous and shoots for conifers).

LAI(CC): this is the LAI calculated with the CC clumping index. The α and γ used are shown in the *.tab file, they are 0 and 1 (defaults), respectively for this example.

LAI(LX): LAI with clumping index from LX clumping index method.

LAI(CLX): LAI with clumping index from CLX clumping index method.

CI(CC): clumping index using the CC method.
CI(LX): clumping index using the LX method.
CI(CLX): clumping index using the CLX method.

OPENNESS(X-Y): Integration of the gap fraction, using Miller, of the gap fraction from view zenith angle X to Y:

$$O = \int_X^Y P(\theta)\sin\theta \mathrm{d}\theta \qquad \textbf{(4.1)}$$

Crown Closure: fraction of the foliage vertical projection, averaged from PAIe for angles less than VZA of 25°.

5. Detailed Theory (based on TRAC manual 2.1.4)

5.1 Leaf Area Index (LAI)

The LAI is defined as one half of the total leaf area per unit ground surface (Chen and Black, 1992; Lang 1991). The major advantage of this definition over the definition based on the projected (one-sided) area (Ross 1981) is that when the foliage angular distribution is random, the usual projection coefficient of 0.5 can still be used for object of any shape. Since foliage elements are oriented in various directions in plant canopies, the projected area in one direction does not contain all the information for estimating radiation interception. The use of half the total area, which in effect is twice the average projected area for all leaf inclination angles, avoids this problem.

Many optical instruments measure canopy gap fraction based on radiation transmission through the canopy. The substantial difference between the LAI measured with these instruments and TRAC is perhaps better understood with the following expression (based on Nilson, 1971):

$$P(\theta) = e^{-G(\theta)\Omega(\theta)L_t / \cos(\theta)} \qquad (5.1)$$

where $P(\theta)$ is the gap fraction, $G(\theta)$ is the foliage projection coefficient characterizing the foliage angular distribution (see Warren Wilson and Reeve, 1959, or Norman and Campbell, 1989, for expressions of $G(\theta)$ with foliage inclination); L_t is the plant area index (PAI) including leaf and woody material; and $\Omega(\theta)$ is a parameter determined by the spatial distribution pattern of the foliage elements. When the foliage spatial distribution is random, $\Omega(\theta)$ is unity. If leaves are regularly distributed (extreme case: leaves are all laid side by side), $\Omega(\theta)$ is larger than unity. When leaves are clumped (extreme case: leaves are stacked on top of each other), $\Omega(\theta)$ is less than unity. Foliage in plant canopies are generally clumped, hence $\Omega(\theta)$ is referred as the clumping index.

Equation (5.1) can be inverted for the plant area index as:

$$L_t = -\frac{\ln[P(\theta)]}{\Omega(\theta)G(\theta)}\cos(\theta) \,. \qquad (5.2)$$

$P(\theta)$ can be easily measured and the next section will show how $\Omega(\theta)$ is estimated. The problem in using equation 5.2 is that $G(\theta)$ is not known and is difficult to measure. In the case of randomly oriented foliage elements, $G(\theta) = 0.5$. Many canopies can be approximated by a random foliage orientation, but Warren Wilson and Reeve (1959) showed that for any foliage orientation, near the view zenith angle of one radian (57.3°), $G(\theta)$ is always near 0.5. Thus Eq. (5.2) can be used near 57.3° within the knowledge of the foliage orientation. Another solution is the use of Miller theorem (1967). Miller showed that for any foliage orientation probability distribution,

$$\int_0^{\pi/2} G(\theta)\sin\theta \mathrm{d}\theta = 0.5 \,. \qquad (5.3)$$

Isolating $G(\theta)L_t$ in Eqs. (5.1) and integrating using the relation from (5.3) yields (Fernandes *et al.*, 2001):

$$L_t = -2\int_0^{\pi/2} \frac{\ln[P(\theta)]}{\Omega(\theta)}\cos(\theta)\sin\theta \mathrm{d}\theta \qquad (5.4)$$

Equation 5.4 implies that the gap fraction and clumping index have to be measured from 0 to 90 degrees. Conifer needles are grouped at several levels: shoots, branches, whirls and tree crowns, and even groups of trees. Conifer shoots (the basic collection of needles distributed around the smallest stem) are treated as the basic foliage units affecting radiation transmission (Norman and Jarvis, 1975; Ross et al., 1986; Oker-Blom, 1986; Leverenz and Hinkley, 1990; Gower and Norman, 1990; Fassnacht et al., 1994). Chen and Black (1992b) and Chen and Cihlar (1995a) determined from canopy gap size distributions that the size of the basic foliage unit is the average projected shoot width.

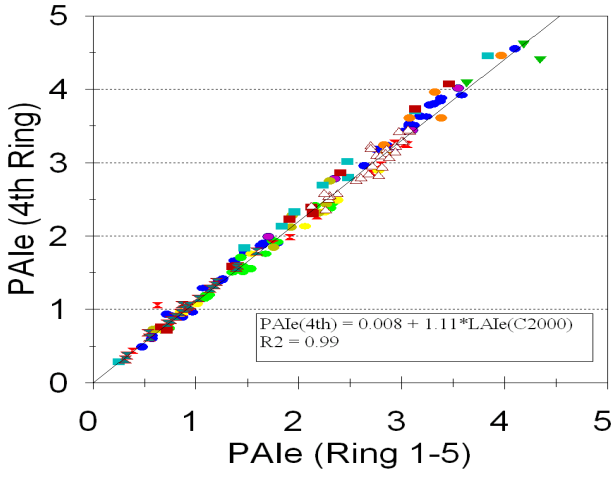

Figure 5.1: Comparison between effective PAI (PAIe) retrieved using five annulus rings (0-74°) and from only one ring (47-58°). The fit is almost perfect (R^2=0.99) with a systematic increase due to either multiple scattering in the fifth ring (Leblanc and Chen, 2001; Leblanc et al., 2002) or clumping more pronounced at low view zenith angles

(Leblanc et al., 2005). The measurements are from different species in Ontario and Quebec (see Chen *et al.*, 2002).

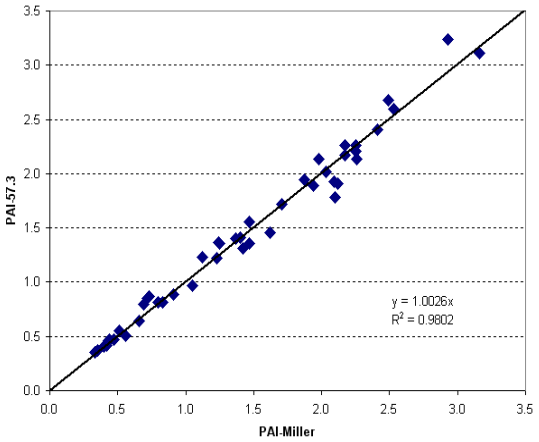

Figure 5.2: Similar to 5.1, but from DHP measurements and clumping corrected.

This is because small gaps disappear in the shadow in a short distance as a result of the penumbra effect. Therefore it is difficult to measure the amount of needle area within the shoots with optical instruments and the Ω(θ) value has to be separated into two components as follows (Chen, 1996a):

$$\Omega(\theta) = \frac{\Omega_E(\theta)}{\gamma_E}, \qquad (5.6)$$

where γ_E is the needle-to-shoot area ratio quantifying the effect of foliage clumping within a shoot (it increases with increasing clumping) and $\Omega_E(\theta)$ includes the effect of foliage clumping at scales larger than the shoot (it decreases with increasing clumping).

The needle-to-shoot area ratio is used to quantify foliage clumping within shoots. Fassnacht *et al*. (1994) proposed an equation for calculating the shoot area, which is an improvement over the method of Gower and Norman (1990). Chen (1996a) developed the following equation to calculate one half of the total shoot area (A_s), which differs slightly from Fassnacht *et al.* (1994):

$$A_s = \frac{1}{\pi}\int_0^{2\pi} d\Phi \int_0^{\pi/2} A_p(\theta,\Phi)\cos\theta d\theta, \qquad (5.7)$$

where θ is the zenith angle of projection relative to the shoot main axis, and Φ is the azimuthal angle difference between the projection and the shoot main axis. A shoot having an equal projected area at all angles of projection can be approximated by a sphere. In such a case A_s, half the total shoot imaginary surface area, equals 2 times the projected area. If one half of the total area (all sides) of needles in a shoot is A_n, then

$$\gamma_E = A_n / A_s \qquad (5.8)$$

For deciduous forests, individual leaves are considered as the foliage elements and γ_E=1.

Kucharik *et al.* (1997; 1999) explored the importance of the angular variation of $\Omega_E(\theta)$. They proposed the following equation to get the clumping index at different θ:

$$\Omega_E(\theta) = \frac{\Omega_{E,MAX}}{1 + b\exp(k\theta^P)}, \qquad (5.9)$$

where p , b and k are constants, θ is the zenith angle (in radian), The constants are species dependent. Kucharik *et al.* (1999) found through Monte Carlo simulations the following: aspen: p = 3.0 and k = 1.6, and for conifers like jack pine and black spruce: p = 1.72 and k = 2.38.

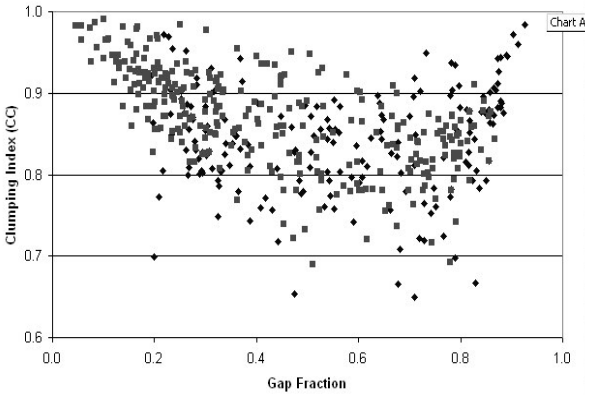

Fig 5.3: Relationship between gap fraction and clumping index. Each point is from a specific plot view zenith angle at 5° interval, ranging from 10 to 80°.

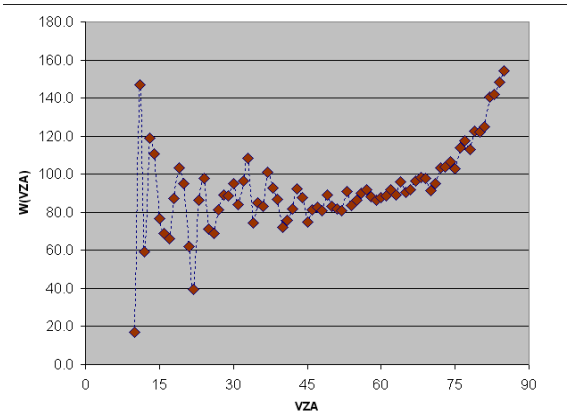

Fig 5.4 W(θ) from loop mode

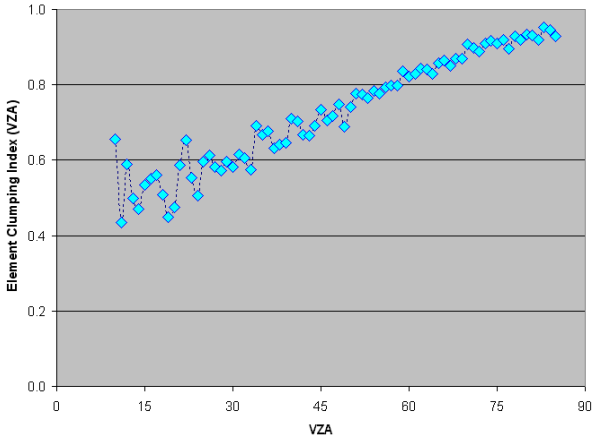

Fig 5.5 Extracted clumping index Ω(θ).

Moreover, Fig. 3.3 shows simulations done with the Five-Scale model (Leblanc and Chen, 2000). The Five-Scale curves include clumping at all scales while Fig. 3.2 includes only the clumping at the scale larger than the shoots. The shape of the Five-Scale curves (Fig. 5.6) is more closely related to the data than Kucharik *et al.* (1999) curves. An approximation of the Five-Scale curves can be obtained with a polynomial of degree three: $\Omega(\theta) = A + B\theta + C\theta^2 + D\theta^3$.

As stated by Kucharik *et al.* (1999), $\Omega(\theta=90) = 1$ since both clumped and random based gap fraction will go to zero, but since the value is not used in the calculation with Miller's equation (sin(90°) =0), it is better not to use that point in a regression to find A, B, C and D. Moreover, simulations using only Beer's law show that the curve can be in opposite trend (see Fig. 5.7)

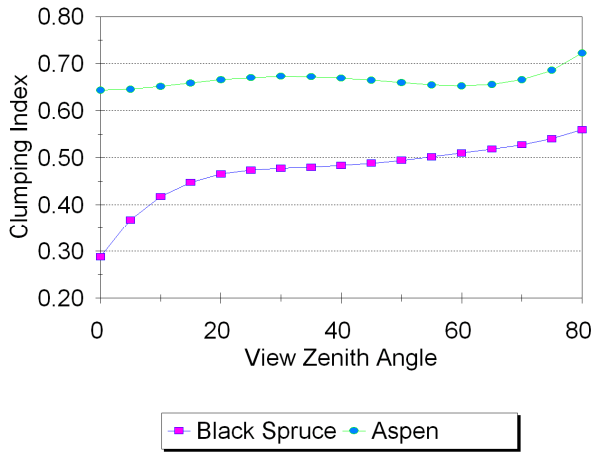

Figure 5.6: Five-Scale Simulations of the clumping index versus the view zenith angle for two boreal forests (from Leblanc and Chen, 2002). The clumping index for the simulated black spruce stand includes the clumping of needles in shoots.

Since L_t is obtained from gap fraction measurements, and is the quantity that many optical instruments measure, Chen (1996a) used it as a basis for calculating LAI using the following equation:

$$L = L_t(1-\alpha) \tag{5.10}$$

where α is the woody-to-total area ratio.

Since L_t is usually measured near the ground surface based on radiation transmission, all above-ground materials, including green and dead leaves, branches, and tree trunks and their attachments (lichen, moss), intercept light and are included in L_t. By using the factor $(1-\alpha)$, the contributions of non-leafy materials are removed. However, the removal using this simple parameter assumes a non-woody material has a spatial distribution pattern similar to that of leaves quantified by Ω(θ).

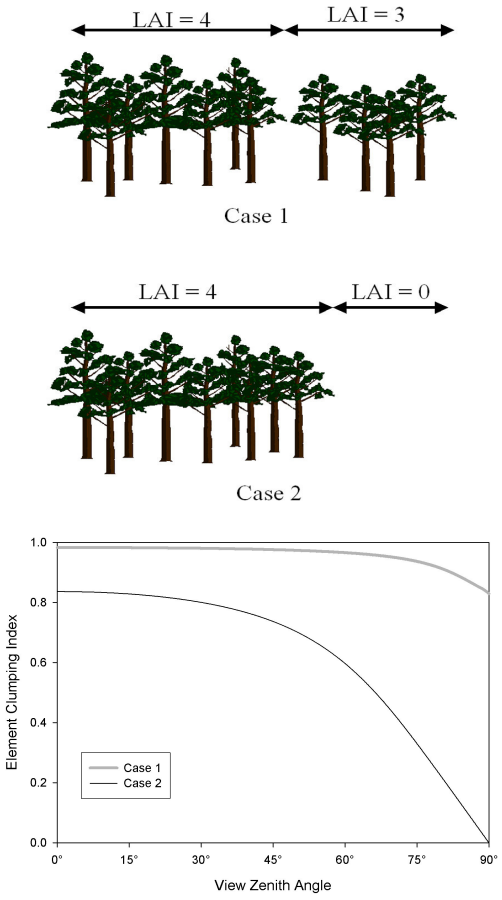

Figure 5.7: Theoretical cases, both with LAI of 3.6, where the clumping index decreases with increasing view zenith angle due to case 1: a stand with two random LAI segments and case 2: due to a large opening (LAI =0).

This assumption may result in a small error in the LAI estimation. The value of α is obtained through destructive sampling (Chen, 1996a) or from measurements taken before leaf emergence of after leaf-off (Chen *et al.*, 1997b; Leblanc and Chen, 2002). New ways of estimating α have been investigated using a two-band camera (Kucharik et al., 1997). The remaining task in obtaining LAI is to determine $\Omega(\theta)$.

5.2 Measurements of LAI and foliage clumping index

If foliage elements, i.e., leaves of deciduous canopies and shoots of conifer canopies, are randomly distributed in space, $\Omega(\theta)$ equals unity and only γ_E and α are needed for calculating LAI of conifer canopies from gap fraction estimates. For most plant canopies, foliage elements are clumped, resulting in $\Omega(\theta)$ smaller than unity. When foliage elements are grouped at higher levels, the total gap fraction increases for the same LAI, and so does the probability of observing large gaps. A canopy gap size distribution can therefore used to quantify $\Omega(\theta)$. The TRAC is designed to acquire the gap size distribution through measurements of sunfleck widths along transects beneath the canopy. The corrected equation for calculating $\Omega_E(\theta)$ is (Leblanc 2002)

$$\Omega_E(\theta) = \frac{\ln[F_m(\theta,0)]}{\ln[F_{mr}(\theta,0)]} \cdot \left[1 + \frac{F_m(\theta,0) - F_{mr}(\theta,0)}{\left[1 - F_m(\theta,0)\right]}\right] \quad (5.11)$$

where $F_m(0)$ is the measured total canopy gap fraction, and $F_{mr}(0)$ is the gap fraction for a canopy with randomly positioned elements. While $F_m(0)$ can be measured as the transmittance of direct or diffuse radiation at the zenith angle of interest, $F_{mr}(0)$ is obtained through processing a canopy gap size accumulation curve, $F_m(\lambda)$, which is the accumulated gap fraction resulting from gaps with size l larger than or equal to λ. At $\lambda = 0$, $F_m(\lambda)$ is the total gap fraction as measured by other optical instruments. $F_m(\lambda)$ can be measured. According to Miller and Norman (1971), the pattern of gap size accumulation for a random canopy, denoted by $F_r(\lambda)$, can be predicted from LAI and the foliage element width. By comparing $F_m(\lambda)$ with $F_r(\lambda)$, large gaps appearing at probabilities larger than the prediction of $F_r(\lambda)$ can be identified and removed from the total gap accumulation. $F_{mr}(\lambda)$ is $F_m(\lambda)$ brought to the closest agreement with $F_r(\lambda)$, representing the case of a random canopy with the same LAI. In the calculation of $F_r(\lambda)$, LAI is required, but it is unknown. Chen and Cihlar (1995a) solved the problem by using an iteration method. For a given measured $F_m(\lambda)$, the iteration always converges to a unique value.

In general, for multiple angle measurements at θ_i, i = 1, ... n, the same sin θ weighting scheme can be used, i.e.

$$L_t = -\frac{\sum_{i=1}^{n} \frac{2}{\Omega(\theta_i)} \cos(\theta_i)\sin(\theta_i)\ln\left(P(\theta_i)\right)}{\sum_{i=1}^{n} \sin(\theta_1)} \quad (5.12)$$

Eq. (5.4) can be used to get *Lt* from multiple angular gap fraction measurements with Eq. (5.4) being the discrete approximation. If the summation is done over the range 0 to 90°, eliminating the need for the assumption of random distributed foliage. An alternative is to invert at the angle θ_E:

$$L_t = -\frac{2\cos(\theta_E)\ln\left(P(\theta_E)\right)}{\Omega(\theta_E)} \quad (5.13)$$

The reasons for using a θ_E at 57.3° can be seen in Leblanc and Chen (2001) that showed that PAI*e* near in the range 48-58° is always close to PAI*e* from Miller's theorem (see Fig. 3.1). This has been known for a long time (Warren Wilson, 1960) but not often used.

5.3 Details of gap theory

The theory presented here follows Chen and Cihlar (1995a) with modifications by Leblanc (2002) and adaptation to hemispherical photographs by Leblanc et al., (2005).

If a canopy is homogeneous at large scales, gap measurements over a length more than 10 times longer than the average tree spacing can statistically represent the canopy with an accuracy of 95% according to the Poisson probability theory. Otherwise, they represent only part of the canopy measured. Naturally, gaps vary irregularly in size.

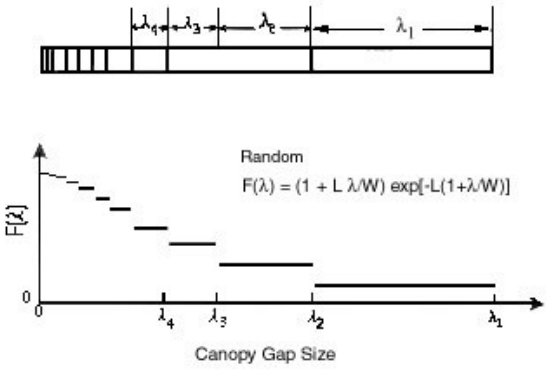

Figure 5.8 Schematic canopy gap size distribution measure on a transect beneath the canopy, where F(λ) is the fraction of the transect that is occupied by gaps larger than λ.

For the data analysis, the measured gaps are rearranged in an ascending or descending order by their size and a gap size accumulation function $F(\lambda)$ can thus be formed (Figure 5.6), where $F(\lambda)$ denotes the fraction of the transect occupied by gaps larger than λ. In Figure 3.4, $F(\lambda) = 0$ for λ values larger than λ_1 since no gaps are found to be larger than λ_1. If λ_1 is the only gap on the transect of length L, $F(\lambda)$ in Figure 5.6 would appear to be a horizontal line from 0 to λ_1 at a value of λ_1/L. Since many smaller gaps exist, $F(\lambda)$ increases as λ decreases. At $\lambda = 0$, $F(\lambda)$ becomes the fraction of the transect occupied by all gaps, i.e., the total gap fraction of the canopy.

5.3.1 Random Canopy

Miller and Norman (1971) showed that for a canopy with horizontal leaves randomly distributed in space and the sun at zenith, $F(\lambda)$ is determined as follows:

$$F(\lambda) = (1 + \rho w \lambda) e^{-\rho(\sigma + w\lambda)} \qquad (5.14)$$

where ρ is the number of leaves per unit ground surface area, σ is the area of a leaf, and w is the average width of leaves in the direction perpendicular to the transect. Following the methodology used by Chen and Black (1992b), Eq. (5.14) can be rewritten as

$$F(\lambda) = (1 + L\frac{\lambda}{W}) e^{-L(1+\lambda/W)} , \qquad (5.15)$$

where $L = \rho\sigma$, i.e. the leaf area index, and W is the characteristic width of a leaf, defined as

$$W = \frac{\sigma}{w} . \qquad (5.16)$$

Since σ is proportional to w^2, W is proportional to w, i.e.

$$W = cw , \qquad (5.17)$$

where c is a constant depending on the shape of the leaves. For circular disks, w is the diameter and $c = \pi/4$.

For conifer stands, shoots are identified as the basic foliage units or elements (please refer to Results). To apply Eq. (5.15) to plant canopies with the sun at a non-zero zenith angle and non-horizontal foliage elements, several modifications need to be made. First, L is to be replaced by L_p (projected L_E) defined as

$$L_p(\theta) = \frac{G(\theta) L_E}{\cos\theta} , \qquad (5.18)$$

where $G(\theta)$ is the projection coefficient determined by the incident angle θ and the distribution of the foliage element normal, being 0.5 for a random (spherical) distribution of the normal. The term $1/\cos\theta$ compensates for the path length of a beam passing through the canopy at a given angle θ, and L_E is the foliage-element area index. Here the distinction between L and L_E is made. If leaves are treated as the elements, L_E is the leaf area index L; but if shoots are identified as elements, L_E becomes the shoot area index (assuming $L_E = L/\gamma$).

The second modification to Eq. (5.15) is to replace W with $W_p(\theta)$. $W_p(\theta)$ is the mean width of the foliage element projected on a horizontal surface and is defined as

$$W_p(\theta) = \frac{\overline{W}}{\cos\theta} \qquad (5.19)$$

where $\overline{W}$ is the mean width of an element projected on a plane perpendicular to the direction of pixel view. The term $1/\cos\theta_p$ in this equation takes into account the elongation of the element on a horizontal plane in the direction of the measuring transect. θ_p, which may be termed the "width projection angle", depends on the shape of the element and the azimuthal angles of the sun and the transect. After these modifications, Eq. (5.15) becomes

$$F(\lambda,\theta) = \left[1 + L_p(\theta)\frac{\lambda}{W_p(\theta)}\right] e^{-L_p(\theta)[1+\lambda/Wp(\theta)]} \qquad (5.20)$$

5.3.2 Non-random Canopies

The spatial distribution of foliage elements (e.g. shoots) is seldom random, and therefore any measured distribution (denoted $F_m(\lambda)$) in a plant canopy is very unlikely to overlap with $F(\lambda)$ for canopies with random foliage distributions. Foliage in plantations and natural forest stands are generally clumped, resulting in larger canopy gap fractions than those of random canopies with the same LAI. When a canopy is clumped, not only the gap fraction increases but also the gap size distribution changes. This change can be shown as the difference between $F(\lambda,\theta)$ and $F_m(\lambda,\theta)$. Therefore the difference provides information on the foliage spatial distribution in a canopy. A new method is developed in this study to derive the element clumping

index from a measured gap size distribution. The clumping index $\Omega_E(\theta)$ is given in the following equation:

$$P(\theta) = e^{-G(\theta)\Omega_E(\theta)L_E/\cos\theta} \quad (5.21)$$

where $P(\theta)$ is the penetration probability of at an incidence angle through the canopy without being intercepted. This equation demonstrates that canopy gap fraction measurements by the PCA or other optical instruments only provide information for the calculation of $\Omega_E L_E$ rather than L if $\Omega_E(\theta)$ is unknown. By definition, $P(\theta)$ equals the canopy gap fraction in the same direction, i.e. $P(\theta) = F_m(0,\theta)$ at θ. Therefore

$$\Omega_E(\theta)L_E = -\frac{\cos\theta}{G(\theta)}\ln[F_m(0)] \quad (5.22)$$

If we know an equivalent $F(\lambda)$ for a canopy, i.e. the gap size distribution where the foliage elements are randomly spaced ($\Omega_E(\theta) = 1.0$), we have

$$L_E = -\frac{\cos\theta}{G(\theta)}\ln[F(0)] \quad (5.23)$$

where $F(0)$ is $F(\lambda)$ at $\lambda = 0$. Combining Eqs. (3.28) and (3.29) results in

$$\Omega_E(\theta) = \frac{\ln[F_m(0,\theta)]}{\ln[F(0,\theta)]} \quad (5.24)$$

This equation states that the clumping index can be calculated from the measured gap fraction $F_m(0,\theta)$ and an imaginary gap fraction $F(0,\theta)$ for a canopy with a random spatial distribution of the foliage elements. It will be demonstrated here that the random canopy gap fraction $F(0,\theta)$ can be derived from a measured gap size distribution $F_m(\lambda,\theta)$.

To find $F(0,\theta)$, it is necessary to know $F(\lambda,\theta)$ (Eq. 5.20), which requires input of the element size $W_p(\theta)$ and the projected element area index L_p defined in Eq. (5.18). For broad-leaf canopies, $W_p(\theta)$ can be taken as the average leaf width, but for needle-leaf canopies, it is questionable to treat needles as the foliage elements. Gower and Norman (1990) and Fassnacht *et al.*, (1994) made corrections to the PCA measurements based on the assumption that shoots of conifers are the basic foliage units responsible for radiation interception. Deblonde *et al.* (1994) also used this approach. From sunfleck size distributions in a Douglas-fir stand, Chen and Black (1992) derived an element size, which is slightly larger than the characteristic size of the shoots. These findings are consistent with visual observations that needles are closely grouped in shoots that appear to be distinct units of foliage. Section 5.4 shows how TRACWin derives the foliage element size based on Chen and Black's method.

To determine L_p, it is required to know L_E (Eq. 5.23), but L_E is also unknown. However, a measured gap size distribution $F_m(\lambda)$ helps solve the problem. When a canopy is clumped (such as conifer stands where the spatial positions of shoots are confined within individual branches and tree crowns), large canopy gaps appear, i.e. the gaps between tree crowns and branches are generally larger than those within these structures. In other words, large gaps are more frequently observed in clumped canopies than in random canopies. These large gaps increase the canopy gap fraction and therefore affect the indirect measurements of LAI. If we know the probability of the appearance of large gaps for a random canopy, i.e., $F(\lambda,\theta)$, given the values of W_p and L_p, we can remove the effect of these large gaps on LAI measurements by removing them from the total gap fraction. As the value of L_p is unknown, we first use $\Omega_E L_E$ as L_E, i.e. L_p is first taken as $-\ln[F_m(0)]$ from Eqs. 5.18 and 5.20, to produce the first estimate of $F(\lambda,\theta)$. Gaps appearing at probabilities in excess of $F(\lambda,\theta)$ are then removed or truncated. After the first round of gap removal, a new gap size distribution $F_{mr}(\lambda,\theta)$ is computed. In the second step, L_p is assigned the value of $-\ln[F_{mr}(0,\theta)]$, which is larger than its first estimate because $F_{mr}(0,\theta)$ is smaller than $F_m(0,\theta)$.

The final value of L_p is found after several iterations of the same steps until no increase in L_P is found, i.e. the new distribution $F_{mr}(\lambda,\theta)$ becomes closely overlapped with $F(\lambda,\theta)$.

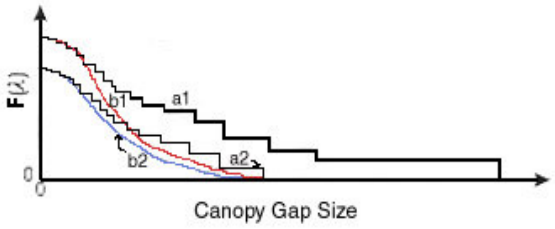

Figure 5.9: Gap-size distributions and re-distributions after two gap removal processes where a1 is a measured gap-size distribution, b1 is the first estimate of the distribution for a random canopy, a2 is the redistribution after the two largest gaps are removed, b2 is the second estimate. In finding the final distribution for the calculation of the clumping index. The process is repeated until the distribution is brought to the closet agreement with the distribution for a random canopy.

Fig. 5.9 demonstrates the changes in $F_{mr}(\lambda,\theta)$ with the iterations. Curve a1 is the measured distribution $F_m(\lambda,\theta)$ and curve b1 is a predicted distribution $F_r(\lambda,\theta)$ for the case of random foliage distribution using measured W_p and the first estimate of L_p. The non-randomness of the canopy is seen from the difference in curves a1 and b1: many large gaps appear at probabilities much larger than $F_r(\lambda,\theta)$. After some of the excessive gaps are removed, the first estimate of $F_{mr}(\lambda,\theta)$ is formed as curve a2 and the second $F_r(\lambda,\theta)$, curve b2, is obtained using the same W_p but different L_p obtained from $F_{mr}(\lambda,\theta)$, ensuring $F_r(0,\theta) = F_{mr}(0,\theta)$. In the operation, when a gap of size λ_i is removed, $F_{mr}(\lambda,\theta)$ at all λ values smaller than λ_i is reduced by λ_i/L_t. This makes the curve $F_m(\lambda,\theta)$ shifts downward by the same amount. Curves a2 and b2 still exhibit large differences, and further removal of the remaining large gaps is still needed. Since in the random case there is always a non-zero probability for the appearance of a gap of however large size, a small portion of a truncated gap remains. Many such partial truncations makes $F_{mr}(\lambda,\theta)$ smoother after each iteration.

The iteration stops when either the increase in L_P becomes very small or a portion of $F_{mr}(\lambda,\theta)$ falls below $F_r(\lambda,\theta)$. The later case happens more often because measured distributions at small λ values always deviate to some extent from the ideal random conditions. Fig. 5.10 illustrates the rationale for the gap removal approach. Assuming an originally random canopy is split into many sections with gaps inserted between them, these "foreign" gaps increase the gap fraction and make the apparent foliage area available for radiation interception smaller

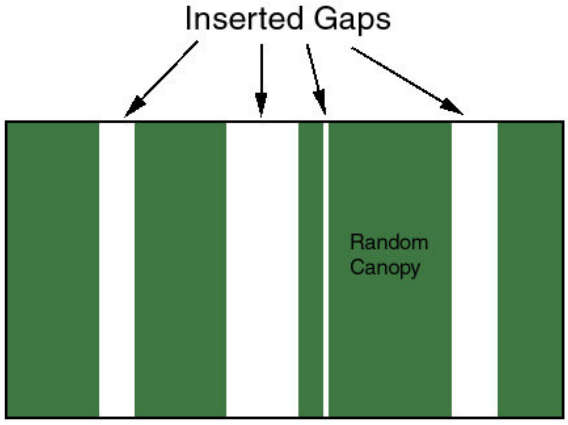

Figure 5.10. Gap removal approach to reconstructing a random canopy for LAI calculations. Large gaps between foliage clumps (crowns, branches, etc) are considered to be "inserted" non-random gaps.

The gap removal process discussed above can therefore be regarded as a reversal of the gap insertion process, which restores the random state of the canopy. Since in a random canopy, the gap size distribution follows a predictable pattern, these foreign gaps can be identified in a measured gap size distribution. In reality, the separated pieces with local randomness do not exist, and gaps resulting from foliage clumping are mixed with gaps that exist in random canopies. Therefore the "insertion" of gaps depicted in Fig. 5.10 is not a realistic case. However, the gap size analysis method presented above does NOT require the assumption of the local randomness because only the gaps resulting from foliage clumping are removed and the gaps appearing at probabilities in accord with $F_r(\lambda,\theta)$ are kept. In other words, in the gap removal process, the foliage elements are computationally rearranged in space to form a random canopy.

After the removal or truncation of large gaps the canopy becomes compacted, i.e. the ground surface area it occupies is reduced by the total fraction of gaps (Δg) removed (Leblanc 2002)

$$\Delta g = \frac{F_m(0,\theta) - F_{mr}(0,\theta)}{1 - F_m(0,\theta)}. \qquad (5.25)$$

By definition, the element area index for the compacted canopy is

$$L_{Ec}(\theta) = -\frac{\cos\theta}{G(\theta)} \ln[F_{mr}(0,\theta)]. \qquad (5.26)$$

If the elements are redistributed in the original total area, i.e. the compacted canopy area is expanded by Δg, the element area index after the expansion is

$$L_E(\theta) = -\frac{\cos\theta}{(1+\Delta g)G(\theta)} \ln[F_{mr}(0,\theta)]. \qquad (5.27)$$

From Eqs. (3.28) and (3.33), it can be shown that

$$\Omega_E(\theta) = \frac{\ln[F_m(0,\theta)]}{\ln[F_{mr}(0,\theta)]}(1+\Delta g) \qquad (5.28)$$

After the gaps removal, $F_{mr}(0,\theta)$ equals $F_r(0,\theta)$. $F_r(0,\theta)$ differs from $F(0,\theta)$ because of the canopy compaction is not considered in $F(0,\theta)$. Eq. (5.28) is a slight modification to Eq. (5.24) to consider the compactness of the canopy involved in the gap removal. The total gap fraction $F_m(0,\theta)$ can be accurately measured as the transmittance of direct light through the canopy. The accuracy in the calculated $\Omega_E(\theta)$ values lies largely in determining $F_{mr}(0,\theta)$ from a measured gap size distribution.

5.4 Gap Size distribution model (The "*P*" approach)

The *P* approach (see Chen and Cihlar, 1995b) is described here to show how the element size can be computed from the TRAC measurements.

The following formula describes the gap size distribution of a canopy with random spatial distribution of foliage elements:

$$P(\lambda,\theta) = e^{-L_p(\theta)[1+\lambda/W_p(\theta)]} \qquad (5.29)$$

When plotting ln(P[λ,θ]), the intercept is -L_p and the slope at zero is L_p(θ)/W_p(θ). Which can be used to calculated W_p(θ). W_p(θ) estimated from the measurements are usually larger than from foliage sampling. The *PFL file has the W estimate at each λ. The W Loop added to TRACWin is used to find the W_p(θ)p from a random canopy gap size distribution. The loop removes the gaps in an iterative way. First to find a F_{mr}(0,θ) and P_{mr}(0,θ) based on the W_p(θ) measured from the non-random canopy. Then a second time from this reduced canopy, a new W_p(θ) is calculated and the reduction is done a second time. Two reduction is usually sufficient for F_{mr}(0,θ) and W_p(θ) to converge.

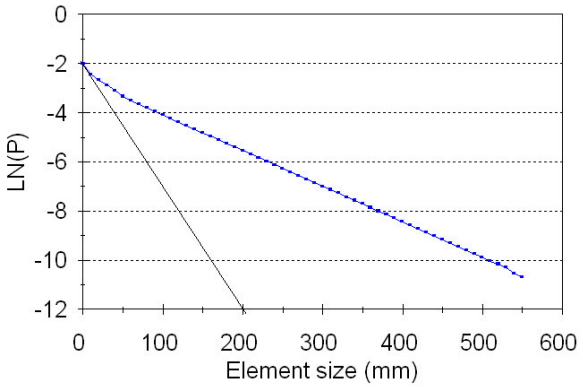

Figure 5.11: In this plot, L_p = 1.996 and the slope at 0 is -0.04434 which gives a W_p of 45 mm. The typical width (W) for that forest was about 35 mm based on sampled leaves. The random part of the curve (constant slope) has an element width of 183 mm which could represent the clumping of leaves in branches. See Chen and Cihlar (1995b) for more details on the "P" approach. If the operator walks too fast, small gaps won't be visible and W_p computed may be larger than the actual foliage typical width.

6.0 Gamma Correction

Digital cameras have CCD that measure photon. A count of photon through a canopy is linearly related to the gap size. However, the human eye does not see light in a linear fashion, thus to have a photograph that looks like what the human eye would see, a correction is applied to the original digital numbers: a gamma correction (see Cescatti A., 2006):

$$DN = MAX\left(\frac{DN}{MAX}\right)^{\Gamma} \qquad (6.1)$$

Equation 6.1 will still have DNs between 0 and 255, but the image usually looks darker than the one with the gamma correction. Gamma correction is often seen on monitor adjustment and image processing software (e.g. Photoshop) to improve image viewing on different monitor. For example, Macintosh and PCs are known to use different gamma values. Making images appear darker on some systems. Gamma correction is also used simultaneously with radiometric reduction. Many digital cameras now have a radiometry depth of more than 8-bit per colour. The raw image is transformed within the camera into a format such as jpeg using proprietary factors. However, the Γ value itself is generally 2.2

The DHP analysis requires the original DN count, before the gamma correction, to perform gap size estimates. This fact was not considered in previous DHP version (prior to version 4.0). New digital cameras have a raw mode that, in theory, has the original DN value before any corrections such as the gamma correction, but those file format cannot be read directly by DHP.exe. If the gamma correction factor (Γ) is not known, we suggest using Γ = 2.2 as default (sRGB mode). Γ usually varies between 2 and 2.5 for natural looking photographs.

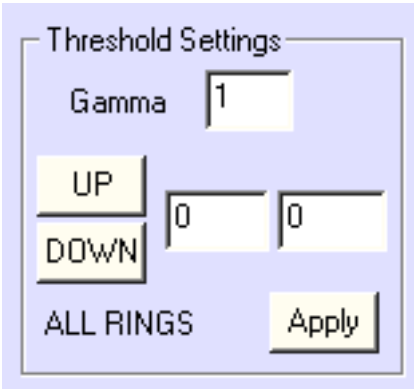

Figure 6.1: DHP now has a gamma correction value input. It is used only when applying the thresholds.

7.0 Batch mode

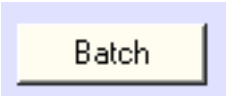

Fig. 7.1 Batch button

The batch mode is still limited. It was developed to use with simulated hemispherical photographs that can be analysed using fixed thresholds. Future versions may allow batch analysis with more flexibility. The batch file needs to be saved in the directory where hemi-photos are saved. Note that all images with the extension (file type) choose (e.g. bmp) will be analysed, whether they are hemispherical photograph or not. The batch parameters are the same as normal hemispherical analysis. The image size is read when opening the files and the colour channel is decided from the main interface.

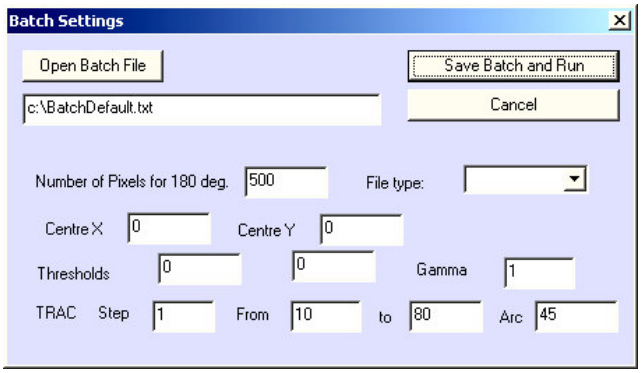

Figure 7.1 Batch Settings Dialog box.

8.0. List of symbols

Name	Acronym	Symbol
Leaf Area Index	LAI	L
Plant Area Index	PAI	L_t
Effective Leaf Area Index	LAIe	$L_e(\theta)$
Effective Plant Area Index	PAIe	$L_{et}(\theta)$
Woody Material Area Index	WAI	M
Effective Woody Material Area Index	WAIe	$M_e(\theta)$
Foliage Clumping Index from all scales	FCI	$\Omega(\theta)$
Total Clumping Index from all scales	TCI	$\Omega_T(\theta)$
Foliage element Clumping Index	FCI_E	$\Omega_E(\theta)$
Woody Material Clumping Index	WCI	$\Omega_W(\theta)$
Needle to shoot ratio (clumping at scale smaller than shoot)	-	γ_E
Foliage Element Projection coefficient	-	$G(\theta)$
Apparent Foliage Element Projection coefficient ($=G(\theta)\Omega_E(\theta)$)	-	$G_A(\theta)$
Zenith Angle; Solar Zenith Angle; View Zenith Angle	ZA; SZA; VZA	θ; θ_s; θ_v
Equivalent Miller's theorem (view or solar) Zenith Angle	ZA_E	$\theta_E \sim 57.3$
Sunlit leaf area index	-	L_{su}
Shaded leaf area index	-	L_{sh}
Woody to total plant area index	-	α

9.0. References and Suggested Reading

Anderson, M. C., 1964. Studies of the woodland light climate I. The photographic computation of light condition. Journal of Ecology 52:27-41.

Beets, P., 1977. Determination of the fascicle surface area for Pinus Radiata. New Zeal. J. For. Sci. 7:397-407.

Bonan, G. B., 1993. Importance of leaf area index and forest type when estimating photosynthesis in boreal forests. Remote Sensing of Environment 43:303-314.

Bonhomme, R., C. Varlet Granger, and P. Chartier, 1974. The use of hemispherical photographs for determining the leaf area index of young crops. Photosynthetica 8:299-301.

Brand, D.G., 1987. Estimating the surface area of spruce and pine foliage from displaced volume and length. Can. J. For. Res. 17:1305-1308.

Cescatti A., 2006. Indirect estimates of canopy gap fraction based on the linear conversion of hemispherical photographs. Methodology and comparison with standard thresholding techniques. Agric. For. Meteorol. (in press)

Chen, J. M., 1996a. Optically based methods for measuring seasonal variation in leaf area index of boreal conifer forests. Agricultural and Forest Meteorology, 80:135-163.

Chen, J. M., 1996b. Canopy architecture and remote sensing of the fraction of photosynthetically active radiation in boreal conifer stands. IEEE Transactions on Geoscience and Remote Sensing, 34:1353-1368.

Chen, J.M., T. A. Black and R. S. Adams, 1991. "Evaluation of hemispherical photography for determining plant area index and geometry of a forest stand." Agric. for Meteorol., 56: 129-143.

Chen, J. M., P. M. Rich, T. S. Gower, J. M. Norman, S. Plummer, 1997. "Leaf area index of boreal forests: theory, techniques and measurements". Journal of Geophysical Research, 102(D24):29,429-29,444.

Chen, J.M. and T.A. Black, 1991, Measuring leaf area index of plant canopies with branch architecture", Agri. and For. Meteor. vol. 57, pp. 1-12.

Chen, J.M. and T.A. Black, 1992a, Defining leaf area index for non flat leaves, Plant Cell Environ., vol. 15, pp. 421-429.

Chen, J. M., and T. A. Black, 1992b, Foliage area and architecture of plant canopies from sunfleck size distributions. Agric. For. Meteorol. 60: 249-266.

Chen, J. M. and J. Cihlar, 1995a. Plant canopy gap size analysis theory for improving optical measurements of leaf area index. Applied Optics, 34:6211-6222.

Chen, J. M. and J. Cihlar, 1995b. Quantifying the effect of canopy architecture on optical measurements of leaf area index using two gap size analysis methods. IEEE Transactions on Geosciences and Remote Sensing, 33:777-787.

Chen, J. M., and J. Cihlar, 1996. Retrieving Leaf Area Index of Boreal Conifer Forests Using Landsat TM Images, Remote Sensing of Environment, Vol. 55, pp. 153-162.

Chen, J. M. and S.G. Leblanc, 1997. "A Four-Scale Bidirectional Reflection Model Based on Canopy Architecture". IEEE Transactions on Geoscience and Remote Sensing, 35:1316-1337.

Chen, J. M., P. D. Blanken, T. A. Black, M. Guilbeault and S. Chen, 1997a. Radiation regime and canopy architecture in a boreal aspen forest. Agric. For. Meteorol. 86:107-125.

Chen, J. M., G. Pavlic, L. Brown, J. Cihlar, S. G. Leblanc, H. P. White, R. J. Hall, D. Peddle, D.J. King, J. A. Trofymow, E. Swift, J. Van der Sanden, P. Pellikka, 2001. Derivation and Validation of Canada-wide coarse-resolution leaf area index maps using high resolution satellite imagery and ground measurements. Remote Sensing of Environment (in press)

Clark, D.B., D.A. Clark, P.M. Rich, S.B. Weiss, and S.F. Oberbauer, 1996, Landscape-scale evaluation of understory light and canopy structure: methods and application in a neotropical lowland rain forest. Canadian Journal of Forest Research 26:747-757.

Evans, G. C., and D. E. Coombe, 1959, Hemispherical and woodland canopy photography and the light climate. Journal of Ecology 47:103-113.

Fassnacht, K., S. T. Gower, J. M. Norman, and R. E. McMurtrie, 1994, A comparison of optical and direct methods for estimating foliage surface area index in forests. Agric. For. Meteorol. 71:183-207.

Fernandes R., H.P. White, S. G. Leblanc, G. Pavlic, H. McNairn, J.M. Chen, D. King, E. Seed, I. Olthof, R. Hall

Examination of Error Propagation in Relationships between Leaf Area Index and Spectral Vegetation Indices from Landsat TM and ETM. 23rd CSRS, Quebec City, August 21-24, 2001.

Galo, A.T., P.M. Rich, and J. J. Ewel, 1992, Effects of forest edges on the solar radiation regime in a series of reconstructed tropical ecosystems. American Society for Photogrammetry and Remote Sensing Technical Papers. pp 98- 108.

Gower, S. T., and J. M. Norman, 1990, Rapid estimation of leaf area index in forests using the LI COR LAI 2000. Ecology 72:1896-1900.

Gower, S.T., J.G. Vogel, J.M. Norman, C. J. Kucharik, S.J. Steele, and T.K. Stow, 1997, Carbon distribution and aboveground net primary production in aspen, jack pine, and black spruce stands in Saskatchewan and Manitoba, Canada. J. Geophys. Res. 102(D24): 29,029-29,041.

Gower S. T., Kucharik J. K., and Norman J. M., 1999, Direct and Indirect Estimation of leaf area index, fapar, and net primary production of terrestrial ecosystems. Remote sens. environ. 70: 29-51.

Grier, C.C., K.M. Lee, and R.M. Archibald, 1984, Effects of urea fertilization on allometric relations in young Douglas-Fir trees. Can. J. For. Res. 15:900-904.

Johnson, J.D., 1984, A rapid technique for estimating total surface area of pine needles. Forest Sci. 30:913-921.

Jonckheere, I., Nackaerts, K., Muys, B. and Coppin, P. 2005. Assessment of automatic gap fraction estimation of forests from digital hemispherical photography. Agric. For. Meteorol. Vol. 132, pp. 96-114.

Kucharik, C. J., J. M. Norman, L. M. Murdock and S. T. Gower, 1997. Characterizing canopy nonrandomness with a Multiband Vegetation Imager (MVI). J. Geophy. Res.vol. 102, No. D24, pp. 29,455-29,473.

Kucharik, C. J., J. M. Norman, and S. T. Gower, 1999. Characterization of radiation regimes in nonrandom forest canopies: theory, measurements, and a simplified modeling approach. Tree Physiology, 19: 695-706.

Lang, A.R.G, and Y. Xiang, 1986, Estimation of leaf area index from transmission of direct sunlight in discontinuous canopies Agric. For. Meteor. 35, 229-43.

Lang, A. R. G., 1991, Application of some of Cauchy's theorems to estimation of surface areas of leaves, needles and branches of plants, and light transmittance. Agric. For. Meteorol. 55: 191-212.

Leblanc, S. G. 2002. Correction to the plant canopy gap size analysis theory used by the Tracing Radiation and Architecture of Canopies instrument. Applied Optics, Vol. 31, No. 36, 7667-7670

Leblanc S. G., and J. M. Chen 2000. A Windows Graphic Interface (GUI) for the Five-Scale Model for fast BRDF Simulations. Remote Sensing reviews, vol. 19, pp. 293-305.

Leblanc, S. G. and J. M. Chen, 2001, A practical scheme for correcting multiple scattering effects on optical LAI measurements, Agric. For. Meteorol. 110: 125-139.

Leblanc, S. G., J. M. Chen, H. P. White, J. Cihlar, R. Lacaze, J.-L. Roujean, and R. Latifovic, 2001a, Mapping Vegetation Clumping Index from Directional Satellite Measurements. Proceeding of 8th International Symposium Physical Measurements and Signatures in Remote Sensing, Aussois, 8-12 January 2001. PP. 450-459

Leblanc S. G., S. Wang, R. Fernandes, H. Peter White, J. M. Chen. 2001b. Implication of foliage spatial and angular distributions in environmental studies. 23rd CSRS, Quebec City, August 21-24, 2001.

Leblanc S. G., Chen J. M., Kwong M. 2002. Tracing Radiation and Architecture of Canopies (TRAC) MANUAL Version 2.1, Canada Centre for Remote Sensing, Natural Resources Canada , 25 p.

Leblanc, S. G., Chen, J. M., Fernandes, R., Deering, D. a and Conley, A., 2005. Methodology comparison for Extraction of plant canopy structure parameters from digital hemispherical photography in boreal forest. Agric. For Meteorol., Vol. 129. pp. 187-207. 2005

Leverenz, J. W., and T. M. Hinckley, 1990, Shoot structure, leaf area index and productivity of evergreen conifer stands. Tree Physiology 6:135-149.

Lerdau, M.T., N. M. Holbrook, H.A. Mooney, P.M. Rich, and J.L. Whitbeck, 1992, Seasonal patterns of acid fluctuations and resource storage in the arborescent cactus Opuntia excelsa in relation to light availability and size. Oecologia 92:166-171.

Lin, T., P.M. Rich, D.A. Heisler, and F.J. Barnes, 1992, Influences of canopy geometry on near-ground solar radiation and water balances of pinyon-juniper and ponderosa pine woodlands. American Society for

Photogrammetry and Remote Sensing Technical Papers. pp. 285-294.

Miller, J.B. 1967. "A Formula for average foliage density." Aust. J. Bot., 15: 141-144.

Miller, E. E. and J. M. Norman, 1971. "A sunfleck theory for plant canopies. I length of sunlit segments along a transect". Agronomy Journal, 63:735-738

Mitchell, P.L., and T.C. Whitmore, 1993, Use of hemispherical photographs in forest ecology: calculation of absolute amount of radiation beneath the canopy. Oxford Forestry Institute. Oxford, United Kingdom.

Nilson T., 1971 A theoretical analysis of the frequency of gaps in plant stands. Agric. For Meteorol., 8:25-38.

Nilson T., 1999. Inversion of gap frequency data in forest stands. Agric. For Meteorol. 98-99:437-448.

Norman J. M. and G. S. Campbell, 1989, "Crop canopy photosynthesis and conductance from leaf measurements" Workshop prepared for LI-COR, Inc., Lincoln, NE (From Welles, J.M. (1990) Some indirect methods of Estimating Canopy Structure in: eds Goel, N.S. and Norman, J.M. Instrumentation for studying vegetation canopies for remote sensing in optical and thermal infrared region, remote sensing review, 5: 31-43, 1988

Norman, J. M. and P. G. Jarvis, 1975, Photosynthesis in Sitka spruce (Picea sitchensis (Bong.) Carr.) III measurement of canopy structure and interception of radiation. J. Appl. Ecol. 11:375-398.

Neumann, H. H., G. den Hartog, and R. H. Shaw, 1989, Leaf area measurements based on hemispheric photographs and leaf-litter collection in a deciduous forest during autumn leaf-fall. Agric. For. Meteorol., 45: 325-345.

Oker-Blom, P., 1986, Photosynthetic radiation regime and canopy structure in modeled forest stands. Acta For. Fenn. 197:1-44.

Pearcy, R.W., 1989, Radiation and light measurements. pp. 95-116. In: R.W. Pearcy, J. Ehleringer, H.A. Mooney, and P.W. Rundel (eds), Plant Physiological Ecology: Field Methods and Instrumentation. Chapman and Hall. New York. 762-1767.

Rich, P.M., 1989, A manual for analysis of hemispherical canopy photography. Los Alamos National Laboratory Report LA-11733-M.

Rich, P.M., 1990, Characterizing plant canopies with hemispherical photographs. In: N.S. Goel and J.M. Norman (eds), Instrumentation for studying vegetation canopies for remote sensing in optical and thermal infrared regions. Remote Sensing Reviews 5:13-29.

Rich, P.M., D.A. Clark, D.B. Clark, and S.F. Oberbauer, 1993, Long-term study of solar radiation regimes in a tropical wet forest using quantum sensors and hemispherical photography. For. Meteorol. 65:107-127.

Rich, P.M., J. Chen, S.J. Sulatycki, R. Vashisht, and W.S. Wachspress, 1995, Calculation of leaf area index and other canopy indices from gap fraction: a manual for the LAICALC software. Kansas Applied Remote Sensing Program Open File Report. Lawrence, KS.

Ross 1981, "The Radiation regime and architecture of plan stands." Dr. W. Junk Publishes

Ross, J. S. Kellomaki, P. Oker-Blom, V. Ross and L. Vilikainen, 1986. Architecture of Scots pine crown: Phytometrical characteristics of needles and shoots. Silva Fennica 19:91-105.

Running, S. W., and J. C. Coughlan, 1988, A General Model of Forest Ecosystem Processes for Regional Applications I. Hydrological Balance, Canopy Gas Exchange and Primary Production Processes", Ecological Modelling, Vol. 42, pp. 125-154.

Sellers, P. J., Y. Mintz, Y. C. Sud, and A. Dalcher, 1986, A simple biosphere model (SiB) for use within general circulation models, J. Atmos. Sci. 43:505-531.

Stenberg, P., S. Linder, H. Smolander and J. Flower-Ellis, 1994, Performance of the LAI-2000 plant canopy analyzer in estimating leaf area index of some Scots pine stands. Tree Physiology 14:981-995.

Walter, J.M., Fournier, R. A., Soudani, K, Meyer, E., 2003. Intehrating clumping effects in forest canopy structure: an assessment through hemispherical photographs. Can. J. Remote Sens. 29(3), 388-410.

Walter, J.M., and Torquebiau E. F. 2000. The computation of forest leaf area index on slope using fish-eye sensors, Comptes Rendus de l'Académie des Sciences - Series III - Sciences de la Vie Volume 323, Issue 9 , September 2000, Pages 801-813

Van Gardingen, G.E., Jackson, G.E., Hermandez-Daumas, S., Russell, G., and Sharp, L., 1999. Leaf Area index estimates obtained for clumped canopies using hemispherical photography. Agric. For. Meteor. 94, 243-257.

Wagner, S., 1998. Calibration of grey values of hemispherical photographs for image analysis. Agri. For. Meteorol. 90, 103-117.

Wagner, S., 2001. Relative radiance measurements and zenith angle dependent segmentation in hemispherical photography. Agri. For. Meteorol. 107: 103–115

Vogel, J. 1997, Carbon and nitrogen dynamics of boreal jack pine stands with different understory vegetation. M. Sc. Thesis, University of Wisconsin, Madison, WI.

Warren-Wilson, J., and J.E. Reeve. (1959). Analysis of the spatial distribution of foliage by two-dimensional point quadrats. New Phytol. 58: 92-101.

Warren Wilson, J., 1965, Stand structure and light penetration, I. Analysis by point quadrats. J. Appl. Ecol., 2: 383-390.

Welles, J.M., 1990. Some indirect methods of estimating canopy structure. Remote Sensing Reviews 5:31-43.

Special thanks to Jing Chen, Alexis Conley, Alain Demers, Richard Fernandes, Richard Fournier, Gordon Frazer, John Iiames, Doug King, Craig Macfarlane, Natasha Neumann, Ian Olthof, Drew Pilant, Jeff Privette, Steve Tuyl, Peter White and many others for your questions and comments about DHP and TRACWin.